Experimental Study of $\bar{p}n$ Annihilation Cross Sections in $\bar{p}d$ Interactions between 1.0 and 1.6 GeV/c

R. H. Huesman

Lawrence Berkeley Laboratory

University of California

Berkeley, California

25 April 1974

TABLE OF CONTENTS

Experimental Study of $\bar{p}n$ Annihilation Cross Sections in $\bar{p}d$ Interactions between 1.0 and 1.6 GeV/c

R. H. Huesman

Lawrence Berkeley Laboratory

University of California

Berkeley, California

25 April 1974

ABSTRACT

A systematic study of $\bar{p}n$ annihilations into three or more pions has been performed in the region of the enhancement in the I=1, $\bar{N}N$ total cross section at 2190 MeV. Cross sections are reported for the final states $\pi^+2\pi^-$, $\pi^+2\pi^-\pi^0$, $\pi^+2\pi^-(m\pi\geq 2\pi^0)$, $2\pi^+3\pi^-$, $2\pi^+3\pi^-\pi^0$ and $2\pi^+3\pi^-(m\pi\geq 2\pi^0)$. Assuming the enhancement is due to a resonance, a simple model is used to estimate the amount of resonance present in each final state. The fits result in some resonance in all final states, and at the 95% confidence level, non-zero lower limits exist for the final states $\pi^+2\pi^-$, $\pi^+2\pi^-\pi^0$ and $2\pi^+3\pi^-$.

I. INTRODUCTION

In a high statistics counter experiment, Abrams et. al.[1] measured the $\bar{p}p$ and $\bar{p}d$ total cross sections between 1.0 and 3.3 GeV/c incident beam momentum. In their resulting unfolded I=1, $\bar{N}N$ total cross section, shown in figure (1), they observed two bumps at 1.32 GeV/c and 1.77 GeV/c over a smooth background of about 100 mb. Assuming that each of the bumps is a result of a single resonance, their fits to the I=1 total cross section gave the following Breit-Wigner parameters:

a) m = 2190 MeV, Γ = 85 MeV and height 5.5 mb.;

b) m = 2350 MeV, Γ = 140 MeV and height 3.2 mb.

We shall refer to these two structures as the T and U-mesons respectively.[2]

We report a study of the $\bar{p}d$ interactions at nominal $\bar{p}$ beam momenta of 1.0, 1.1, 1.2, 1.3, 1.4, 1.5 and 1.6 GeV/c. This experiment is a collaborative effort between various members of four laboratories located at Padova, Pisa, Torino and Berkeley,[3] and was designed to study the pure I = 1, $\bar{p}n$ interactions in the T-meson region. The beam momenta were chosen to give overlapping $\bar{p}n$ center of mass energy when the Fermi momentum of the neutron in the deuteron is taken into account. The exposure consisted of 370,000 pictures in the CERN 81 cm. deuterium filled bubble chamber. The film was scanned at Padova, Pisa and Torino, and a selected sample of events was measured and processed at Berkeley. The processed data has been analyzed at all four labs.

We have already reported on preliminary work done on the $\bar{p}n$ partial cross sections,[4] on the structure in the $\bar{p}n \to \pi^+ 2\pi^-$ Dalitz plot[5] and on the $\bar{p}n \to \bar{N}N\pi\pi$ cross sections.[6] This report concerns the topological cross sections and the reaction cross sections for $\bar{p}n$ annihilations.

The broad bump at m ≈ 2190 MeV (the T-meson) observed by Abrams et. al.[1] has been confirmed in the $\bar{p}p$ total cross section with the Rutgers Annihilation Spectrometer.[7] From bubble chamber data for single-pion production in $\bar{p}p$ and $\bar{p}n$ interactions, it has been shown that the bump is not caused by the $\bar{N}N\pi$ channel.[6,8-10] In a $\bar{p}p$ bubble chamber experiment Kalbfleisch et. al. have reported evidence for an enhancement in the $\rho^0\rho^0\pi^0$ channel at 2190 MeV.[11] In another $\bar{p}p$ bubble chamber experiment Donald et. al., in disagreement with Kalbfleisch et. al, find no structure in the $\rho^0\rho^0\pi^0$ channel.[12] There are several recent reviews of the experimental situation.[13-15]

Assuming that the T-meson is an s-channel resonance of the $\bar{N}N$ system, we shall study the $\bar{p}n$ annihilations into pions in order to determine if it decays into any of these final states. The $\bar{p}n$ system is a pure I=1 state which makes this type of analysis favorable. A disadvantage is that we must extract $\bar{p}n$ cross sections from $\bar{p}d$ interactions and correct for the effects of the deuteron.

The details of the scan, including total and topological cross sections is discussed in section II. In section III we describe the processing of events used to determine the $\bar{p}d$ cross sections for reactions with three or more charged particles in the final state in addition to a final state proton which stops in the bubble chamber. Section IV considers the problem of extracting $\bar{p}n$ cross sections from $\bar{p}d$ data, and in section V we discuss the relation between these cross sections and the T-meson. Section VI gives our conclusions derived from this analysis, the main conclusion being that no one final state is responsible for the enhancement known as the T-meson.

II. THE SCAN

Our definition of topologies is illustrated in figure (2). Even prong events in which one of the prongs is a dark stopping track are called odd prongs in this scheme; the dark track is a low momentum proton which can be identified as a "spectator" of the $\bar{p}n$ interaction.

The film was scanned for all interactions within a specified fiducial volume of the bubble chamber, and the total number of entering beam tracks was counted. The effort of scanning was divided between Padova, Pisa and Torino. For all momentum settings except 1.0 GeV/c each of the three labs scanned approximately one third of the film. The 1.0 GeV/c film was all scanned at Torino. In addition about 14% of the 1.2 GeV/c film was rescanned at Padova. Table (1) gives the number of interactions and beam tracks found in the first scan.

By counting δ rays on the beam tracks and noting how many of the beam tracks with δ rays interact in the bubble chamber, we have determined that at 1.0 and 1.2 GeV/c the beam was contaminated with 6.2% μ's and 3.5% π's. At the other momentum settings a different beam transport was used, and in these runs the beam contamination was less than 0.5%. At 1.0 and 1.2 GeV/c we decrease the number of beam tracks by 9.7%, and using known π and topological cross sections, we correct the scan numbers for the corresponding topologies accordingly.

From the second scan performed at Padova, we have calculated scan efficiencies for all topologies except the 1-prongs which are considered in the next paragraph. Scan efficiencies are about 93% for all topologies except 0-prongs for which the scan efficiency is 81%. It was found that interactions

which were classified as 0-prongs on the first scan did not change topology on the second scan. This was not true for other topologies however, and the efficiency for counting all interactions together (which were not 0-prongs) was found to be 96%. We increased the number of 0-prongs by the factor 96/81 for all beam momenta and all labs, although the scan efficiencies were calculated only for 1.2 GeV/c events scanned at Padova. We have not determined the efficiency of counting beam tracks, but we shall assume that it is also 96%. This is probably an underestimate, but will only lead to a scale error.

In a study performed at Padova, the 1-prong losses in the forward direction have been evaluated by an extrapolation of the distribution of events vs. lab scattering angle projected onto the scan table. It is estimated that the number of 1-prong events lost in the forward direction is 10±2% of the total number of events found in the first scan and is independent of beam momentum over our range. Due to differences in the scanning, we use 10.6±2% and 7.9±2% to correct for 1-prong losses in the film scanned at Pisa and Torino respectively. These numbers were determined by requiring that the average resulting fractions of 1-prongs be the same as for Padova.

Table (2) gives the corrected numbers of events and beam tracks (all with a constant scan efficiency of 96%, for which no correction has been made). Total cross sections based on the corrected scan numbers for each of the three labs separately are shown in figure (3). The errors shown include a 2% error added in quadrature to the statistical errors to account for uncertainties in the 1-prong corrections. The statistical errors vary between 0.3% and 1.0%, so that the uncertainties in the 1-prong corrections dominate and give rise to the large error bars shown. For comparison, we also show on

figure (3) the more accurately determined total cross section of Abrams et. al.[1] The agreement is good.

For the purpose of calculating topological cross sections, we normalize our total cross sections for each lab at each momentum separately to the $\bar{p}d$ total cross section of Abrams et. al.[1] This is done to minimize the effect of the unknown efficiency in counting beam track. Table (3) gives the topological cross sections which are a weighted average of the normalized cross sections from the three labs.

As can be seen in figure (3), the cross section of Abrams et. al has a four or five millibarn bump at 1.3 GeV/c. The bump arises from the I=1, $\bar{N}N$ cross section enhancement at 2190 MeV (the T-meson) which has been smeared out due to the Fermi motion inside the deuteron. The bump in the $\bar{p}d$ cross section is only a few per cent of the total, and the renormalization of our data introduces no bump which was not already there.

III. MEASUREMENT AND EVENT SEPARATION

All events of the 3-prong and 5-prong topologies were selected for measurement on the spiral reader and processed through the POOH-TVGP-SQUAW chain. It is impossible to determine whether small angle 1-prong events are $\bar{p}n$, $\bar{p}p$ or $\bar{p}d$ interactions. We do not consider reactions from the 1-prong topology in this report. Each event was tested for consistancy with all hypotheses listed in table (4) appropriate to its topology. Events failing to have a successful fit or missing mass calculation were remeasured and reprocessed one time. The overall passing rate was about 80% for 3-prongs and 70% for 5-prongs. Events not successfully processed fall into one of the following catagories:

a) 17% of the failures were spiral reader operator rejects (wrong event type, wrong beam track or event not on the frame).

b) 21% of the failures were due to the inability of the filter program to find the correct track images.

c) 11% of the failures had a track which had large point scatter or could otherwise not be reconstructed.

d) 24% of the failures had a measured beam momentum which was not consistant with a value previously determined for each momentum setting. (This will occur if the beam particle has scattered before entering the bubble chamber.)

e) 10% of the failures were due to spiral reader operator errors. They had no track which was flagged stopping by the spiral reader operator, but hey were scanned as events with a stopping proton.

f) 17% of the failures had measurements which were inconsistant with

energy and momentum balance for all hypotheses tested.

g) 3% of the events, after having passed successfully through the chain, were rejected for having had a track for which the momentum could not be adequately determined resulting in a reduction of the number of constraints. (This was deemed necessary since missing mass calculations are not possible for such events.)

From a study of the first and second measurements with successful fits or missing mass calculations, we have determined that the combined measurement and processing efficiency is independent of the particular reaction within a given topology for events with spectator proton momenta less than 150 MeV/c. There are two reasons for using this subsample of events. First, we expect these events to be much less contaminated with events in which the proton participated strongly in the interaction. Second, longer proton tracks have a higher probability of being scattered. Since we demand momentum from range for the proton track (unless it is too short to be visible) events with higher proton momenta have a different failure rate. In what follows we shall be referring to the subsample of events with spectator proton momenta less than 150 MeV/c unless we explicitly state otherwise.

Appendix A outlines the selection criteria used to separate events into their most probable hypotheses on an event-by-event basis. It was found that ambiguities between the final states $p_s\pi^+2\pi^-\pi^0$ vs. $p_s\pi^+2\pi^-(mm\pi)$ and $p_s2\pi^+3\pi^-\pi^0$ vs. $p_s2\pi^+3\pi^-(mm\pi)$ could not be reliably resolved on an event-by-event basis. [p_s indicates a stopping proton and $(mm\pi)$ indicates missing neutrals with invariant mass greater than the mass of a π^0.] A statistical separation was made between these final states using the missing mass squared and its error from each event within a given range ($mm^2 < 0.3$

GeV^2 for the 3-prongs and $mm^2 < 0.2\ GeV^2$ for the 5-prongs). All events with larger mm^2 are assumed to belong to the missing mass catagories. A maximum likelihood fit was performed which optimized three parameters:

a) the π^o mass,

b) the number of $\bar{p}d \to p_s \pi^+ 2\pi^- \pi^o$ (or $p_s 2\pi^+ 3\pi^- \pi^o$) events and

c) the number of $\bar{p}d \to p_s \pi^+ 2\pi^- (mm\pi)$ events with $mm^2 < 0.3\ GeV^2$ (or $p_s 2\pi^+ 3\pi^- (mm\pi)$ events with $mm^2 < 0.2\ GeV^2$].

The experimental value of the π^o mass is included as a parameter in the fit since small systematic errors in the beam momentum or spectator momentum may bias the resulting missing mass calculation. The theoretical spectrum to which we fit the data is made up of a delta function at the square of the fitted π^o mass and a Lorentz invariant phase space approximation to the $2\pi^o$ invariant mass squared distribution of the reaction $\bar{p}d \to p_s \pi^+ 2\pi^- 2\pi^o$ (or $\bar{p}d \to p_s 2\pi^+ 3\pi^- 2\pi^o$). We cut the data at $mm^2 = 0.3\ GeV^2$ (or $0.2\ GeV^2$) so that we include all of the single π^o events and still have a simple approximation to the included multi π^o phase space.

In figure (4) we show the combined missing mass squared spectra of the events used in the fits. The superimposed curves represent the expected distributions based on our estimate of the numbers of single π^o and missing mass events. The sharply peaked (large dashed) curve is a sum of Gaussians centered at the fitted π^o mass. For each event with $mm^2 < 0.05\ GeV^2$ a Gaussian with standard deviation equal to the error in mm^2 was added, and finally the curve was renormalized to the fitted number of single π^o events. Similarly, the second (small dashed) curve was obtained by folding Gaussians with our approximation to the $2\pi^o$ invariant mass squared distribution. In this case the Gaussians added had standard deviations equal to the error in mm^2 for the

events with $mm^2 > 0.07\ GeV^2$. The sum of these two curves (the solid curve) is also shown.

Results of the separation of events into various final states are given in table (4). In the tables we have not included numbers for the reaction $\bar{p}d \to p_s p\bar{p}\pi^-$ the details of which have been reported elsewhere.[6] The reader is warned that numbers for the one-constraint and zero-constraint hypotheses with kaons are to be considered as lower limits on the actual numbers of events of this type due to the separation procedure of appendix A. Errors introduced into other final states for this reason are negligible since the cross sections for processes involving kaons are very small.

IV. CROSS SECTIONS FOR THE REACTIONS $\bar{p}n \to \pi$'s

A first approximation to neutron cross sections is obtained by making a simple subtraction of the cross section on protons from the cross section on deuterons. One of the assumptions of this procedure is that the individual proton and neutron cross sections are small compared to the square of the distance between the nucleons.[16] Glauber has evaluated the following first order correction to account for the finite size of these cross sections,[17]

$$\sigma_d = \sigma_p + \sigma_n - \delta\sigma$$
$$\delta\sigma = \sigma_p \cdot \sigma_n \cdot \langle r^{-2} \rangle \cdot (4\pi)^{-1}$$

where $\langle r^{-2} \rangle$ is the average inverse square separation of the nucleons within the deuteron.

The correction term $\delta\sigma$ can be intuitively thought of as a shadow effect on each of the nucleons by interactions of the beam with the other nucleon. The effect is to deplete the flux of the beam particles on each of the nucleons. Because $\sigma_{\bar{p}p}$ and $\sigma_{\bar{p}n}$ are nearly equal throughout our momentum range,[1] we shall correct for the shadow effect by increasing each cross section by the factor,

$$s = (\sigma_{\bar{p}d} + \delta\sigma)/\sigma_{\bar{p}d}$$

Abrams et. al.[1] have evaluated $\delta\sigma$ for $\bar{p}d$ interactions at beam momenta of 1.0 and 1.5 GeV/c to be 24.31 and 20.31 mb. respectively. This gives us two determinations for the factor s within our momentum range (1.117 and 1.112

respectively) which differ by less than 0.5%. We use the average value,

$$s = 1.114$$

Another large effect which cannot be ignored in the extraction of $\bar{p}n$ cross sections from $\bar{p}d$ interactions is the abundance of events with spectator momenta larger than that which is predicted by the deuteron wave function. The abundance of such events causes "feed-up" from our 3 and 5-prongs to our 4 and 6-prongs respectively when long proton tracks leave the bubble chamber. Evidence of this effect is the large difference between our (shadow corrected) 4 and 6-prong cross sections and the 4 and 6-prong cross sections from $\bar{p}p$ interactions,[8,11,18,19] shown in figure (5). In appendix B we compare our even prong topological cross sections with the corresponding $\bar{p}p$ topological cross sections and show that final state scattering of $\bar{p}n$ annihilation products on the spectator proton may be responsible for many of the large momentum protons.

We have made a first order correction for "feed-up" in the following way. Two factors, f_3 and f_5, have been determined such that the quantities,

$$s\cdot(\sigma_4 - f_3\cdot\sigma_3) \text{ and}$$
$$s\cdot(\sigma_6 - f_5\cdot\sigma_5),$$

would be most compatible with the 4 and 6-prong $\bar{p}p$ cross sections respectively. We have determined these two factors to be,

$$f_3 = 0.30$$

$$f_3 = 0.27$$

This finally gives us the following $\bar{p}n$ "topological cross sections" which have been corrected for both the shadow effect and for "feed-up":

$$\sigma(\bar{p}n \to 3\text{-prongs}) = s \cdot (1 + f_3) \cdot \sigma_3$$
$$\sigma(\bar{p}n \to 5\text{-prongs}) = s \cdot (1 + f_5) \cdot \sigma_5$$

Figure (6) shows the effect of these corrections on our 3 and 5-prong cross sections, and table (5) gives the numerical results.

To determine the $\bar{p}n$ reaction cross sections we take the fraction of events in a given final state [from table (4)] and multiply by the corresponding $\bar{p}n$ "topological cross section" [from table (5)]. We present the reaction cross sections for $\bar{p}n \to$'s in table (6). These cross sections are smeared out due to the Fermi motion of the target neutron and the spread in beam momentum. Figure (7) shows a plot of these cross sections vs. beam momentum. The curves are fits to the data which are described in the following section.

V. FITS TO THE T-MESON

We make the tentative assumption that the 5.5 mb. reported by Abrams et. al.[1] is a resonance and use a simple model to estimate how much of it is in the 3 and 5-prong topological cross sections of table (5) and the $\bar{p}n$ pion annihilation cross sections of table (6). We parameterize these reaction cross sections by a suitable background and two Breit-Wigner resonance functions for the T and U-mesons. For the Breit-Wigner's we use the parameters determined by Abrams et. al. in their fit to the unfolded I=1, $\bar{N}N$ total cross section (ie. m=2190 MeV, Γ=85 MeV for the T-meson; m=2350 MeV, Γ=140 MeV for the U-meson).[1] The background we use is $\alpha \cdot p^{-\beta}$, where p(E) is the lab beam momentum corresponding to stationary free neutrons and c.m. energy E. This background is monotonic and positive (for α positive) and corresponds to a linear background on a log-log plot. The parameterized cross section is given by.

$$\sigma(E) = \alpha \cdot p^{-\beta} + a_T \cdot BW(2190,85) + a_U \cdot BW(2350,140)$$

where,

$$p = \{[E^2 - (m_n + m_{\bar{p}})^2][E^2 - (m_n - m_{\bar{p}})^2]/(2m_n)\}^{\frac{1}{2}}$$

$$BW(m,\Gamma) = \Gamma^2/[4(E - m)^2 + \Gamma^2]$$

α, β, a_T and a_U are parameters to be fitted, and m_n and $m_{\bar{p}}$ are the neutron and antiproton masses respectively. The Breit-Wigner function has unit height at the center, so that a_T and a_U are the fitted heights of the T and U-mesons respectively.

The parameterized cross sections are folded with the Fermi motion of

the target neutron and the beam spread and compared with our experimental cross sections of table (6). The details of the folding procedure are given in appendix C. We adjust the parameters to obtain the best fit in the least squares sense. The U-meson may influence some of the fits because it overlaps with the T-meson. We do not expect to be able to determine the amount of U-meson since our range of momenta only allows us to explore up to about 2350 MeV in c.m. energy. Table (7) shows our determination of the amount of T-meson present in each final state as well as the confidence levels of the fits. Figure (7) shows the data with a curve which represents the fit. The dashed curve represents the background term only.

For the more highly constrained events (our four-constraint hypotheses) we can make a better determination of the reaction cross sections. The four-constraint fits give us a rather well determined measurement of the spectator proton momentum (even when it is invisible in the bubble chamber). Therefore we also have a good measurement of the $\bar{p}n$ c.m. energy. Knowledge of the flux of beam particles and the distribution of events as functions of c.m. energy and spectator proton momentum gives us a direct measurement of the unfolded cross section. Further details of this procedure are given in appendix D.

Results of the measurement of the cross sections for the two reactions, $\bar{p}n \to \pi^+ 2\pi^-$ and $\bar{p}n \to 2\pi^+ 3\pi^-$ are shown in figure (8). The curves shown are fits to the cross sections using the same functional form as above. Results of these fits are given in table (8). For comparison we also show in figure (8) the small dashed curves which represent the results of the fits of table (7). The results of the fits of table (8) are compatible with those of table (7), and the parameters of table (8) are better determined. This is because we have used

additional information from each event, although the same events were used.

All of the fits of tables (7) and (8) have acceptable confidence levels. For many of them the fitted amounts of U-meson is larger than the total of 3.2 mb. seen by Abrams et. al.[1] As we stated earlier, the fitted values of a_U do not represent accurate measurements, but we have included a_U as a parameter since the T and U-mesons overlap. The parameters a_T and a_U always have positive correlation, so that if a_U is large we are probably overestimating a_T. The quoted errors of a_T (and a_U) take into account correlations with the other parameters. In what follows an "x standard deviation effect" refers to the statistical significance of the parameter a_T (ie. $x = a_T/\$a_T$).

Looking first at the "$\bar{p}n$ topological cross sections" one may hope to find a clue as to which topology to pursue in search of the decay modes of the T-meson. We have already ruled out the single-pion production as a source of the enhancement, so that we consider only 3-prong annihilations and the total 5-prongs which are all annihilations. The 3-prong annihilations have a 2.3 standard deviation effect, and we may place a lower limit of 1.75 mb. of T-meson present at a confidence level of 95%. In the 5-prongs we have a 2.1 standard deviation effect with a lower limit of 0.04 mb. at a confidence level of 95%. Hence it appears that we should look for decay modes of the T-meson in the 3-prong annihilation reactions. (For completeness we also look at the 5-prong reactions.)

$\underline{\bar{p}n \to \pi^+ 2\pi^-}$

Here we have a four-constraint fit for which we have determined the cross section as a function of c.m. energy. The fit of table (8) gives a 2.1 standard deviation effect, and we have a lower limit of 0.09 mb. of T-meson at a 95% confidence level.

$\bar{p}n \to \pi^+2\pi^-\pi^0$

Of the reactions we have studied, this one has the largest amount of T-meson present. Table (7) shows a 2.0 standard deviation effect, and we place a lower limit of 0.60 mb. of T in this channel at a confidence level of 95%.

$\bar{p}n \to \pi^+2\pi^-(mm\pi)$

This reaction has a 0.8 standard deviation effect and is consistent with no T-meson at a confidence level of 21%.

$\bar{p}n \to 2\pi^+3\pi^-$

Here again we have a four-constraint fit for which we have determined the cross section as a function of c.m. energy. The fit of table (8) gives a 2.0 standard deviation effect and a lower limit of 0.10 mb. of T-meson at 95% a confidence level.

$\bar{p}n \to 2\pi^+3\pi^-\pi^0$ and $\bar{p}n \to 2\pi^+3\pi^-(mm\pi)$

These reactions both have 0.6 standard deviation effects and are consistent with no T-meson at a confidence level of 27%.

We have also combined several reactions of like G-parity and fit them. By combining reactions we have higher statistics, and the determination of the amount of T-meson should be better if the reactions we combine have significant amounts of T.

$\bar{p}n \to \pi^+2\pi^-$ plus $\bar{p}n \to 2\pi^+3\pi^-$

Both of the final states have negative G-parity. Both are four-constraint fits, and we see from table (8) that there is a 2.9 standard deviation effect in their sum. This gives us a lower limit of 0.39 mb. of T-meson present at a confidence level of 95%.

$\bar{p}n \to \pi^+2\pi^-\pi^0$ plus $\bar{p}n \to 2\pi^+3\pi^-\pi^0$

These final states both have positive G-parity, and we see from table (7) that

this combination gives us a 1.9 standard deviation effect for their sum. We place a lower limit of 0.43 mb. of T-meson at a confidence level of 95%. Note that rather than enhancing the accuracy of the determination of the amount of T-meson, we have washed out the more significant effect in $\bar{p}n \to \pi^0 2\pi^- \pi^+$ by adding $\bar{p}n \to 2\pi^0 3\pi^- \pi^+$ which was consistent with no T-meson at all.

VI. CONCLUSIONS

We have presented the results of a systematic study of $\bar{p}n$ annihilations into pions obtained from 3 and 5-prong $\bar{p}d$ interactions in the momentum region 1.0 to 1.6 GeV/c. We have attempted to uncover the source of the 5.5 mb. enhancement in the unfolded I=1, $\bar{N}N$ total cross section known as the T-meson which was observed by Abrams et. al.[1] In a previous paper,[6] we have presented evidence that a threshold effect in the reaction $\bar{p}n \to \bar{p}p\pi^-$ is not responsible for the enhancement, as was originally conjectured by Abrams et. al.[1] This conclusion is substantiated by published $\bar{p}p$ and $\bar{p}n$ single-pion production cross sections from other experiments.[8-10]

In this report we have presented $\bar{p}d$ topological cross sections, "$\bar{p}n$ topological cross sections" for 3 and 5-prongs which have been corrected for the shadow effect and "feed-up" and $\bar{p}n$ reaction cross sections which arise from the 3 and 5-prong topologies. Assuming that the T-meson is an s-channel resonance of the $\bar{p}n$ system, we have attempted to ascertain whether it decays into any of the pion annihilation channels of the 3 and 5-prongs.

The largest effect we have found in a single channel is in the $\pi^+2\pi^-\pi^0$ positive G-parity final state. We have put a lower limit of 0.60 mb. of T-meson in this final state at a confidence level of 95%. We have also found smaller but statistically significant amounts of T-meson in the negative G-parity final states $\pi^+2\pi^-$ and $2\pi^+3\pi^-$. We have put a lower limit of 0.39 mb. of T-meson on the sum of these final states at a confidence level of 95%.

ACKNOWLEDGEMENTS

I would like to thank Ronald Ross, Margaret Garnjost and Frank Solmitz for the guidance they have given me. I would also like to thank our Italian friends who have shouldered most of the load in this collaboration.

I am deeply indebted to my mother and father who provided me with the environment which has fostered my academic pursuits. Most of all I thank my wife Marijean whose moral support and incredible patience have made the completion of this work possible.

This work was supported by the U.S. Atomic Energy Commision.

REFERENCES AND FOOTNOTES

1 R. J. Abrams, R. L. Cool, G. Giacomelli, T. F. Kycia, B. A. Leontic, K. K. Li and D. N. Michael: *Phys. Rev. Lett.*, 18, 1209 (1967); *Phys. Rev.*, D1, 1917 (1970).

2 The names T and U-meson arise from a CERN missing mass spectrometer experiment [G. Chikovani, L. Dubal, M. N. Focacci, W. Kienzle, B. Levrat, B. C. Maglić, M. Martin, C. Nef, P. Schübelin and J. Seguinot: *Phys. Lett.*, 22, 233 (1966)] in which two structures were observed in the same mass positions as, but are much narrower than the structures observed later by Abrams et. al.[1]

3 Istituto di Fisica dell'Universita – Padova
Istituto Nazional di Fisica Nucleare – Sezione de Padova

Istituto di Fisica dell'Universita – Pisa
Istituto Nazional di Fisica Nucleare – Sezione de Pisa

Istituto di Fisica dell'Universita – Torino
Istituto Nazional di Fisica Nucleare – Sezione de Torino

University of California – Berkeley
Lawrence Berkeley laboratory – Berkeley

4 A. Bettini, M. Cresti, M. Mazzucato, L. Peruzzo, S. Sartori, G. Zumerle, M.

Alston-Garnjost, R. Huesman, R. Ross, F. T. Solmitz, A. Bigi, R. Carrata, R. Casali, P. Lariccia, R. Pazzi, G. Borreani, B. Quassiati, G. Rinaudo, M. Vigone and A. Werbrouck: in *Proceedings of the First EPS Conference on "Meson Resonances and Related Electromagnetic Phenomena" - Bologna April 14-16, 1971*, edited by R. H. Dalitz and A. Zichichi (Published by Editrice Compositori, Bologna, Italy), p.353.

5 A. Bettini, M. Cresti, M. Mazzucato, L. Peruzzo, S. Sartori, G. Zumerle, M. Alston-Garnjost, R. Huesman, R. Ross, F. T. Solmitz, L. Bertanza, R. Carrara, R. Casali, P. Lariccia, R. Pazzi, G. Borreani, B. Quassiati, G. Rinaudo, M. Vigone and A. Werbrouck *Nuovo Ciemento*, **1A**, 333 (1971).

6 A. Bettini, M. Cresti, M. Mazzucato, S. Sartori, M. Alston-Garnjost, R. Huesman, R. Ross, F. T. Solmitz, A. Bigi, R. Carrara, R. Casali, P. Lariccia, R. Pazzi, G. Borreani, B. Quassiati, M. Vigone and A. Werbrouck: *Nuovo Ciemento*, **15A**, 563 (1973).

7 J. Alspector, J. K. Cohen, W. C. Harrison, B. Maglich, F. Sannes and D. Van Harlingen: *Phys. Rev. Lett.*, 30, 511 (1973).

8 W. A. Cooper, L. G. Hyman, W. Manner, B. Musgrave and L. Voyvodic: *Phys. Rev. Lett.*, 20, 1059 (1968).

9 T. C. Bacon, I. Butterworth, R. J. Miller, J. J. Phelan, R. A. Donald, D. N. Edwards, D. C. Howard and R. S. Moore: *Nuc. Phys.*, B32, 66 (1971).

10 Z. Ming Ma, J. Mountz, P. Zemany and O. A. Smith: *Nuc. Phys.*, B68, 214 (1974).

11 G. Kalbfleisch, R. Strand and V. Vanderburg: *Phys. Lett.*, 29B, 259 (1969).

12 R. A. Donald, D. N. Edwards, J. K. Gibbins, H. Briand, J. Duboc and F. Levy: *Nuc. Phys.*, B61, 333 (1973).

13 L. Bertanza: in *Symposium on Nucleon-Antinucleon Annihilations – Chexbres March 27-29, 1972*, edited by L. Montanet (CERN 72-10) p.35.

14 R. Diebold: in *Proceedings of the XVI International Conference on High Energy Physics – Batavia September 6-8, 1972*, edited by J. D. Jackson, A. Roberts and R. Donaldson, Vol.3, p.1.

15 O. A. Smith: in *AIP Conference Proceedings, Particles and Fields – Berkeley August 13-17, 1973*, edited by H. H. Bingham, M. Davier and G. R. Lynch, p.163.

16 G. Chew and H. Lewis: *Phys. Rev.*, 84, 779 (1951).

17 R. J. Glauber: *Phys. Rev.*, 100, 242 (1955).

18 R. R. Burns, P. E. Condon, J. Donahue, M. A. Mandelkern and J. Schultz: *Nuc. Phys.*, B27, 109 (1971).

19 R. A. Donald, D. N. Edwards, R. S. Moore, E. J. C. Read, S. Reucroft, A. O. Fredsøen, T. Jacobsen, S. Sire, O. Skjeggestad, P. Saetre, H. Tofte, A. Bettini, S. Limentani, L. Peruzzo, R. Santangelo and S. Sartori: *Nuc. Phys.*, **B6**, 174 (1968).

20 I. J. McGee: *Phys. Rev.*, **151**, 772 (1966).

21 C. Møller: *Kgl. Danske Videnskab. Selskab*, **23**, No.1, Sec.2, p.18ff (1945)

APPENDIX A. SELECTION CRITERIA FOR 3 AND 5-PRONGS

1. Fits are defined as:

   a) four-constraint π-annihilation hypotheses having kinematic confidence level $\geq 10^{-5}$,

   b) other hypotheses without kaons having kinematic confidence level $\geq 10^{-3}$.

   c) hypotheses with kaons having kinematic confidence level $\geq 10^{-2}$.

2. Four classes of fits are put into a hierarchy in the following way (from high to low priority):

   a) all constrained fits except one-constraint fits with kaons,

   b) missing mass calculations without kaons,

   c) one-constraint fits with kaons,

   d) missing mass calculations with kaons.

3. Selection criteria follow:

   a) Take the fit/(missing mass calculation) which has the best kinematic confidence level/(most consistant ionization pulse height) from the class with the highest priority.

   b) The only exception to 3a) is that when the best fit is a one-constraint π-annihilation and the second best fit is a four-constraint π-annihilation, take the four-constraint fit.

   c) After a selection has been made a missing mass cut is made. The event is discarded if missing mass squared (or corresponding missing mass squared) is below minimum. (-0.3 GeV^2 for 3-prongs and -0.2 GeV^2 for 5-prongs)

APPENDIX B. COMPARISON OF $\bar{p}d$ AND $\bar{p}p$ TOPOLOGICAL CROSS SECTIONS

Figures (5a,b) show our (shadow corrected) 4 and 6-prong cross sections along with 4 and 6-prong cross sections from $\bar{p}p$ experiments.[8,11,18,19] We can see that the 4 and 6-prong deuterium cross sections are both high (an excess of $\simeq$ 8 mb. in the 4-prongs and $\simeq$ 3.2 mb. in the 6-prongs) with respect to the hydrogen data. We have investigated several possible explanations for this.

High momentum spectator protons from $\bar{p}n$ interactions may leave the bubble chamber before stopping or not be identified as stopping by scanners and cause "feed-up" from 3 to 4-prongs and from 5 to 6-prongs. This effect should depend to a certain extent on the interaction point and the orientation of the spectator. This hypothesis has been tested by counting the number of spectator protons in the 3 and 5-prong catagories which go toward the inside and the outside of the chamber. An asymmetry exists which favors the protons which go toward the inside of the chamber, but the effect is small compared to our excess of 4 and 6-prong events.

Above a certain momentum, all protons will leave the bubble chamber. The dimensions of the bubble chamber are 50x30x30 cm., and we estimate that on the average, $\bar{p}n$ events with spectators longer than 30 cm. will be "fed-up" to the corresponding even prong topology. This corresponds to a loss of 2.7% assuming the spectator momentum distribution is given by the McGee wave function[13] and leads to the following losses.

$$\sigma_3 \simeq 25 \text{ mb.} \rightarrow .7 \text{ mb. lost to } \sigma_4$$

$$\sigma_5 \simeq 11 \text{ mb.} \rightarrow .3 \text{ mb. lost to } \sigma_6$$

This leaves us with an excess of about 7.3 mb. in the 4-prongs and 2.9 mb. in the 6-prongs.

Secondary particles produced in a $\bar{p}n$ interaction may elastically scatter on the spectator proton giving it enough energy to leave the bubble chamber. This will be particularly favorable for π^+p in the $\Delta(1236)$ resonance region. We now perform an order of magnitude calculation to show that this effect may be responsible for our excess events. The fractions of 3 and 5-prongs "fed-up" are approximately,

$$\Delta\sigma_4/(\sigma_3 + \Delta\sigma_4) = 7.3/32.3 = 23\%$$
$$\Delta\sigma_6/(\sigma_5 + \Delta\sigma_6) = 2.9/13.9 = 21\%$$

Estimating an averge of 6 final state particles, we need about 3.5% probability for any of the final state particles to elastically scatter on the proton and drive it out of the bubble chamber. The average cross section for such a process should be about,

$$\sigma = (.035)(4\pi d^2) = (.035)(4\pi)(2\times10^{-13}\ \text{cm.})^2 = 18\ \text{mb.}$$

where d is the average diameter of the deuteron. Such a cross section does not seem unreasonable for pions on protons. To illustrate the effect we show in figures (9a,b) the total spectrum of π^+p and π^-p masses for the two four-constraint fits, $\bar{p}d \to p_s\pi^+2\pi^-$ and $\bar{p}d \to p_s2\pi^+3\pi^-$ respectively. There is a considerable depletion of events in the π^+p mass region around the $\Delta(1236)$.

To first order, we assume that the 3 and 5-prongs are depleted by

constant factors for "feed-up" over our momentum range. These factors, which are determined in section IV, are

$$f_3/(1 + f_3) = 23\%$$

$$f_5/(1 + f_5) = 21\%$$

"fed-up" from the 3 and 5-prongs respectively. Figure (6) shows the effect of these corrections on our 3 and 5-prong cross sections.

APPENDIX C. FOLDING FERMI MOTION AND BEAM SPREAD WITH $\bar{p}n$ CROSS SECTIONS

Our task here is to take $\sigma(E)$, a $\bar{p}n$ reaction cross section for free neutrons as a function of c.m. energy E, and from it and the properties of the deuteron and of our beam, to determine the $\bar{p}n$ cross section we would measure at one of our nominal beam momenta. We assume that our measured cross section has been properly corrected for the shadow effect and "feed-up" as discussed in section IV. We refer to any one of the measured cross sections of table (7) which are based on the subsample of events with spectator proton momenta less than 150 MeV/c in the lab.

For the distribution of proton momenta within the deuteron we take a distribution derived from the configuration space wave function of McGee.[20] We have normalized this distribution such that its integral from zero to 150 MeV/c is equal to unity. The distribution is denoted by $g(p_p)$, where p_p is the momentum of the spectator proton. The angular distribution of spectator proton momenta is assumed to be isotropic in the lab.

Since the deuteron is at rest in the lab, the antiproton interacts with a neutron which has momentum equal but opposite to that of the spectator proton. The c.m. energy of the $\bar{p}n$ system is taken to be equal to the invariant mass of the system made up of all outgoing particles except the spectator proton, so that the neutron is off-mass-shell. Here we make no correction for off-mass-shell effects.

Since the neutron is not at rest in the lab, the flux of beam particles as observed in the neutron rest frame will vary depending on the magnitude and direction of the velocity of the neutron. We take account of this effect by the

use of a "flux factor".

Following Møller's formulation of a Lorentz invariant cross section,[21] the number of interactions per unit time and per unit volume of target is

$$N = \sigma F$$

where σ is the cross section and

$$F = (\rho_1/E_1)(\rho_2/E_2)[(p_1^\mu p_2^\mu)^2 - (p_1^\mu)^2(p_2^\mu)^2]^{1/2}$$

ρ is the density of particles, E is the energy and p^μ is a four-momentum. The subscripts 1 and 2 refer to the beam and target respectively. The quantities ρ/E are invariants as is the expression in the square bracket. Evaluating F in the rest frame of the target particle we get the familiar result

$$F = (\rho_1/E_1)(\rho_2/E_2)[E_1^2 m_2^2 - m_1^2 m_2^2]^{1/2}$$
$$= \rho_1\rho_2(p_1/E_1) = \rho_1\rho_2 v_1$$

or

$$\sigma = \frac{N/\rho_2}{\rho_1 v_1} = \frac{\#\text{ interactions / target particle / unit time}}{\#\text{ incident particles / unit area / unit time}}$$

where v_1 is the velocity of the beam particles.

The "flux factor" we construct is given by,

$$f(p_{\bar{p}}, p_p, E) = [(p_{\bar{p}}^\mu p_n^\mu)^2 - (p_{\bar{p}}^2)^2(p_n^\mu)^2]^{1/2}(p_{\bar{p}} E_n)^{-1}$$

where $p_{\bar{p}}^\mu$ and p_n^μ are the four-momenta of the antiproton and neutron

respectively, $p_{\bar{p}}$ is the magnitude of the lab momentum of the antiproton and E_n is the lab energy of the neutron. The "flux factor" is simply the flux of beam particles as seen by the moving, off-mass-shell neutron divided by the flux of beam particles as seen by a stationary free neutron. Holding $p_{\bar{p}}$ fixed, $f(p_{\bar{p}}, p_p, E) \to 1$, as $p_p \to 0$.

For interactions with a fixed beam momentum $p_{\bar{p}}$, we would expect to measure the cross section,

$$\sigma'(p_{\bar{p}}) = \int dE\ \sigma(E) \int dp_p\ [E/(2p_{\bar{p}}p_p)]\ f(p_{\bar{p}}, p_p, E)\ g(p_p)$$

where the factor $E/(2p_{\bar{p}}p_p)$ enters as the probability density for having $\bar{p}n$ c.m. energy E, given a beam momentum $p_{\bar{p}}$ and spectator proton momentum p_p. (It is just the Jacobian between $\cos\theta_{\bar{p}n}$ and E multiplied by the probability density for $\cos\theta_{\bar{p}p}$ which is flat.) Figure (10a) illustrates the kinematic limits of E and p_p for $p_{\bar{p}} = 1.3$ GeV/c. In figure (10b) we show the kinematic limits for all of our nominal beam momenta to illustrate the extent of the overlap in E. The theoretical spectator proton momentum spectrum $g(p_p)$ is also shown.

Due to a finite spread in the beam momentum upon entering the bubble chamber and energy lost while passing through the liquid deuterium, we do not have a monochromatic beam. We have calculated the mean value and standard deviation of the distribution of fitted beam momenta from the four-constraint $\bar{p}n$ annihilations into pions. These values were calculated for each nominal beam momentum and are shown in table (9). The distributions of beam momenta were consistant with Gaussian shapes for which the standard deviation of the Gaussian is equal to the standard deviation of the distribution. We shall denote the mean value and standard deviation of one of these distributions by $p^*_{\bar{p}}$ and

δp_β^* respectively.

We finally obtain $\sigma''(p_\beta^*)$ by folding $\sigma'(p_\beta)$ with a Gaussian to take the finite beam spread into account. We therefore have,

$$\sigma''(p_\beta^*) = \int dp_\beta \; \sigma'(p_\beta)\, G(p_\beta, p_\beta^*)$$

$$G(p_\beta, p_\beta^*) = (2\pi)^{-\frac{1}{2}} (\delta p_\beta^*)^{-1} \exp[-\tfrac{1}{2}(p_\beta - p_\beta^*)^2/(\delta p_\beta^*)^2]$$

$\sigma''(p_\beta^*)$ is the cross section we would expect to measure at the nominal beam momentum denoted by p_β^* if the true cross section were given by $\sigma(E)$.

APPENDIX D. DETERMINATION OF REACTION CROSS SECTIONS AS A FUNCTION OF C.M. ENERGY

In this appendix we shall describe the calculation of reaction cross sections as a function of c.m. energy E, when we know the c.m. energy of each event. We shall bin the data into small energy bins ΔE_i centered at E_i. We shall first consider data from only one nominal beam momentum p_β° and generalize to more than one later. We calculate cross sections using the formula,

$$\sigma(E_i) = \frac{n(p_\beta^\circ, E_i)}{\rho_2 \ell(p_\beta^\circ, E_i)}$$

where $n(p_\beta^\circ, E_i)$ is the number of events in the i^{th} energy bin, ρ_2 is the number of deuterons per unit volume and $\ell(p_\beta^\circ, E_i)$ is the pathlength associated with the i^{th} energy bin.

In the spirit of appendix C, we partition the total pathlength $L(p_\beta^\circ)$ at a given nominal beam momentum into the energy bins ΔE_i, in the following manner.

$$\ell(p_\beta^\circ, E_i) = L(p_\beta^\circ) \int_{\Delta E_i} dE\, Q(p_\beta^\circ, E)$$

$$Q(p_\beta^\circ, E) = \int dp_p \int dp_\beta\, [E/(2p_p p_\beta)]\, f(p_\beta, p_p, E)\, g(p_p)\, Q(p_\beta, p_\beta^\circ)$$

where all of these variables have been defined in appendix C, and we use the same notation here. Aside from the "flux factor" $f(p_\beta, p_p, E)$, $Q(p_\beta^\circ, E)$ is just the probability density for the $\bar{p}n$ system to have its c.m. energy equal to E. The "flux factor" takes into account the dependence of the flux of beam particles on the magnitude and direction of the velocity of the neutron.

To combine the results at each of our nominal beam momenta, we sum

the numerator and denominator of the equation for $\epsilon(E_i)$ over nominal beam momentum and get,

$$\epsilon(E_i) = \frac{\sum n(p_s^*, E_i)}{\rho_2 \sum \ell(p_s^*, E_i)}$$

As can be seen from table (4), most of our 3 and 5-prong events are in the one-constraint and zero-constraint categories. For these categories we do not have an accurate measurement of the $\bar{p}n$ c.m. energy, since the spectator proton does not leave a visible track about 70% of the time.

For the four-constraint fits however, the $\bar{p}n$ c.m. energy is well determined although somewhat biased. A proton track which is too short to be seen in the bubble chamber is assigned a measured momentum of zero. For this reason, even the spectator momentum distribution resulting from the four-constraint fits is biased toward zero, and the resulting $\bar{p}n$ c.m. energy spectrum is too narrow. If we relax the three constraints on the spectator proton momentum, we still have a constrained fit which results in a less biased measurement of the $\bar{p}n$ c.m. energy.

We have performed one-constraint fits on the reactions $\bar{p}d \to p_s \pi^+ 2\pi^-$ and $\bar{p}d \to p_s 2\pi^+ 3\pi^-$ in order to determine the $\bar{p}n$ c.m. energy for each event. We have also used a slightly modified spectator proton momentum spectrum for the purpose of partitioning the pathlength. The modification [of $g(p_p)$] takes into account the errors of the fitted values of the proton momentum p_p.

We have described the procedure used to calculate cross sections as a function of c.m. energy. Figure (8) shows the resulting cross sections for the reactions $\bar{p}n \to \pi^+ 2\pi^-$ and $\bar{p}n \to 2\pi^+ 3\pi^-$. Curves shown are fits to the data which are described in section V.

Table (1a) Raw Scan Numbers for Film Scanned at Padova

topology	nominal beam momentum (GeV/c)						
	1.0	1.1	1.2	1.3	1.4	1.5	1.6
0-prongs	0	451	3117	1096	1203	925	981
2-prongs	0	2180	18548	5295	5849	4565	4600
4-prongs	0	2438	20350	6159	6671	5122	5324
6-prongs	0	465	3770	1234	1347	1091	1182
8-prongs	0	10	75	37	29	32	41
1-prongs	0	3908	32771	10212	11007	8355	8263
3-prongs	0	1648	14071	4349	4744	3625	3746
5-prongs	0	715	6223	1971	2046	1638	1689
7-prongs	0	22	177	58	74	49	65
total	0	11837	99102	30411	32970	25402	25891
beam tr.	0	44523	410508	115490	128141	103585	106321

Table (1b) Raw Scan Numbers for Film Scanned at Pisa

topology	nominal beam momentum (GeV/c)						
	1.0	1.1	1.2	1.3	1.4	1.5	1.6
0-prongs	0	531	3194	1093	1103	833	1014
2-prongs	0	2373	16051	5158	5395	4135	4913
4-prongs	0	2746	17348	5993	6058	4548	5444
6-prongs	0	485	3358	1144	1292	1051	1291
8-prongs	0	19	111	33	54	33	60
1-prongs	0	4340	28754	9373	9553	7268	8422
3-prongs	0	1697	11928	4093	4046	3045	3470
5-prongs	0	772	5611	1858	1947	1454	1823
7-prongs	0	28	230	73	78	61	78
total	0	12991	86585	28818	29526	22428	26515
beam tr.	0	49187	362261	111304	117294	92249	110565

Table (1c) Raw Scan Numbers for Film Scanned at Torino

topology	nominal beam momentum (GeV/c)						
	1.0	1.1	1.2	1.3	1.4	1.5	1.6
0-prongs	2073	455	2258	1374	1165	981	1024
2-prongs	8276	1994	9287	5549	4865	4315	4558
4-prongs	9267	2357	9992	6530	5432	4833	5016
6-prongs	1482	374	1745	1128	1093	1055	1078
8-prongs	37	16	53	31	32	29	47
1-prongs	16928	3936	18225	11245	9769	8092	8466
3-prongs	7107	1557	7197	4456	3985	3345	3522
5-prongs	2989	654	3264	1991	1731	1501	1637
7-prongs	101	28	108	63	57	54	58
total	48260	11371	52129	32427	28129	24205	25406
beam tr.	168558	43192	207253	121659	109864	97526	104060

Table (2a) Corrected Scan Numbers for Film Scanned at Padova

topology	nominal beam momentum (GeV/c)						
	1.0	1.1	1.2	1.3	1.4	1.5	1.6
0-prongs	0	540	3615	1312	1440	1107	1174
2-prongs	0	2202	18190	5348	5907	4611	4646
4-prongs	0	2462	20514	6221	6738	5173	5377
6-prongs	0	470	3790	1246	1360	1102	1194
8-prongs	0	10	76	37	29	32	41
1-prongs	0	5151	42664	13412	14479	11034	10994
3-prongs	0	1668	14273	4453	4882	3782	3931
5-prongs	0	722	6285	1991	2066	1654	1706
7-prongs	0	22	179	59	75	49	66
beam tr.	0	44523	370689	115490	128141	103585	103321

Table (2b) Corrected Scan Numbers for Film Scanned at Pisa

topology	nominal beam momentum (GeV/c)						
	1.0	1.1	1.2	1.3	1.4	1.5	1.6
0-prongs	0	629	3668	1295	1307	987	1202
2-prongs	0	2373	15586	5158	5395	4135	4913
4-prongs	0	2746	17315	5993	6058	4548	5444
6-prongs	0	485	3342	1144	1292	1051	1291
8-prongs	0	19	111	33	54	33	60
1-prongs	0	5728	37552	12455	12713	9673	11269
3-prongs	0	1701	11985	4152	4129	3153	3624
5-prongs	0	772	5611	1858	1947	1454	1823
7-prongs	0	28	230	73	78	61	78
beam tr.	0	49187	327122	111304	117294	92249	110565

Table (2c) Corrected Scan Numbers for Film Scanned at Torino

topology	nominal beam momentum (GeV/c)						
	1.0	1.1	1.2	1.3	1.4	1.5	1.6
0-prongs	2446	539	2632	1628	1381	1162	1213
2-prongs	8244	1994	9145	5549	4865	4315	4558
4-prongs	9265	2357	9982	6530	5432	4833	5015
6-prongs	1481	374	1741	1188	1093	1055	1078
8-prongs	37	16	53	31	32	29	47
1-prongs	20738	4841	22240	13832	12014	10028	10499
3-prongs	7103	1561	7244	4520	4063	3459	3667
5-prongs	2989	654	3264	1991	1731	1501	1637
7-prongs	101	28	108	63	57	54	58
beam tr.	166367	43192	196679	121659	109864	97526	104060

Table (3) Topological Cross Sections (mb)

topology	nominal beam momentum (GeV/c)						
	1.0	1.1	1.2	1.3	1.4	1.5	1.6
0-prongs	9.72	8.50	7.38	7.90	7.61	7.33	7.32
	± .47	± .29	± .21	± .23	± .23	± .22	± .22
2-prongs	32.75	32.73	31.99	30.31	29.91	29.54	28.83
	± .76	± .53	± .41	± .42	± .41	± .42	± .41
4-prongs	36.81	37.70	35.51	35.38	33.71	32.91	32.36
	± .84	± .59	± .45	± .48	± .46	± .46	± .44
6-prongs	5.88	6.59	6.56	6.75	6.92	7.25	7.26
	± .20	± .20	± .11	± .14	± .14	± .15	± .15
8-prongs	.15	.21	.17	.19	.19	.21	.30
	± .02	± .03	± .01	± .02	± .02	± .02	± .02
1-prongs	82.38	78.34	76.60	74.92	72.54	69.52	66.95
	±2.42	±1.38	±1.29	±1.29	±1.25	±1.23	±1.21
3-prongs	28.22	24.56	25.00	24.77	24.16	23.47	22.87
	± .67	± .44	± .33	± .36	± .35	± .35	± .33
5-prongs	11.87	10.71	11.32	11.02	10.62	10.42	10.55
	± .33	± .26	± .16	± .19	± .19	± .19	± .19
7-prongs	.40	.38	.37	.36	.38	.36	.41
	± .04	± .04	± .02	± .03	± .03	± .03	± .03

Table (4a) Events of each Hypothesis in the 3-prongs with Spectator Proton Momenta less than 150 MeV/c

reaction	nominal beam momentum (GeV/c)						
	1.0	1.1	1.2	1.3	1.4	1.5	1.6
$\bar{p}d \to p_s \pi^+ 2\pi^-$	256	177	979	430	383	263	252
$\bar{p}d \to p_s \pi^+ 2\pi^- \pi^0$	1168	849	4364	2048	1937	1415	1411
$\bar{p}d \to p_s \pi^+ 2\pi^- (mm\pi)$	2789	2245	12796	5719	5639	4468	4713
$\bar{p}d \to p_s K^+ K^- \pi^-$	39	27	173	66	48	33	50
$\bar{p}d \to p_s K^+ K^- \pi^- \pi^0$ $\bar{p}d \to p_s K^+ K^- 2\pi^- \bar{K}^0$ $\bar{p}d \to p_s \pi^+ K^- \pi^- K^0$	52	37	182	109	76	54	64
$\bar{p}d \to p_s K^+ K^- \pi^- (mm\pi)$ $\bar{p}d \to p_s K^+ 2\pi^- (mmK)$ $\bar{p}d \to p_s \pi^+ K^- \pi^- (mmK)$	32	25	190	82	73	63	69
$\bar{p}d \to p_s p\bar{p}\pi^-$	(see reference 6)						

1. p_s indicates a stopping proton.

2. (mmπ) and (mmK) indicate missing neutrals with invariant mass greater than a π^0 and K^0 respectively.

Table (4b) Events of each Hypothesis in the 5-prongs with Spectator Proton Momenta less than 150 MeV/c

reaction	nominal beam momentum (GeV/c)						
	1.0	1.1	1.2	1.3	1.4	1.5	1.6
$\bar{p}d \to p_s 2\pi^+ 3\pi^-$	381	306	1728	814	754	628	624
$\bar{p}d \to p_s 2\pi^+ 3\pi^- \pi^0$	709	610	3459	1637	1707	1352	1400
$\bar{p}d \to p_s 2\pi^+ 3\pi^- (mm\pi)$	422	360	2282	1046	981	888	980
$\bar{p}d \to p_s K^+ \pi^+ K^- 2\pi^-$	14	14	79	48	46	42	50
$\bar{p}d \to p_s K^+ \pi^+ K^- 2\pi^- \pi^0$ $\bar{p}d \to p_s K^+ \pi^+ 3\pi^- \bar{K}^0$ $\bar{p}d \to p_s 2\pi^+ K^- 2\pi^- K^0$	2	0	15	19	14	12	14
$\bar{p}d \to p_s K^+ \pi^+ K^- 2\pi^- (mm\pi)$ $\bar{p}d \to p_s K^+ \pi^+ 3\pi^- (mmK)$ $\bar{p}d \to p_s 2\pi^+ K^- 2\pi^- (mmK)$	0	1	2	2	2	7	2

1. p_s indicates a stopping proton.

2. (mmπ) and (mmK) indicate missing neutrals with invariant mass greater then a π^0 and K^0 respectively.

Table (5) "Topological Cross Sections" for $\bar{p}n$ (mb)

topology	nominal beam momentum (GeV/c)						
	1.0	1.1	1.2	1.3	1.4	1.5	1.6
3-prongs	40.87	35.57	36.20	35.87	34.99	33.99	33.12
	± .97	± .64	± .48	± .52	± .51	± .51	± .48
5-prongs	16.79	15.15	16.02	15.59	15.02	14.74	14.93
	± .47	± .37	± .23	± .27	± .27	± .27	± .27

Table (6a) Reaction Cross Sections for 3-prongs (mb)

reaction	nominal beam momentum (GeV/c)						
	1.0	1.1	1.2	1.3	1.4	1.5	1.6
$\bar{p}n \to \pi^+ 2\pi^-$	2.41	1.85	1.84	1.72	1.50	1.24	1.08
	± .16	± .14	± .06	± .09	± .08	± .08	± .07
$\bar{p}n \to \pi^+ 2\pi^- \pi^0$	10.98	8.85	8.20	8.21	7.57	6.68	6.02
	± .58	± .47	± .36	± .39	± .36	± .33	± .30
$\bar{p}n \to \pi^+ 2\pi^- (mm\pi)$	26.21	23.41	24.04	22.92	22.05	21.09	20.12
	± .82	± .62	± .48	± .52	± .50	± .49	± .47
$\bar{p}n \to K^+ K^- \pi^-$	.37	.28	.33	.26	.19	.16	.21
	± .06	± .05	± .02	± .03	± .03	± .03	± .03
$\bar{p}n \to K^+ K^- \pi^- \pi^0$							
$\bar{p}n \to K^+ 2\pi^- \bar{K}^0$	.49	.39	.34	.44	.30	.25	.27
$\bar{p}n \to \pi^+ K^- \pi^- K^0$	± .07	± .06	± .03	± .04	± .03	± .03	± .03
$\bar{p}n \to K^+ K^- \pi^- (mm\pi)$							
$\bar{p}n \to K^+ 2\pi^- (mmK)$	.30	.26	.36	.33	.29	.30	.29
$\bar{p}n \to \pi^+ K^- \pi^- (mmK)$	± .05	± .05	± .03	± .04	± .03	± .04	± .04
$\bar{p}n \to p\bar{p}\pi^-$	.12	.54	1.10	1.98	3.10	4.27	5.13
	± .03	± .07	± .04	± .10	± .13	± .17	± .19

1. Cross sections for the reaction $\bar{p}n \to p\bar{p}\pi^-$ have been taken from reference (6) and corrected for the shadow effect and "feed-up".

2. $(mm\pi)$ and (mmK) indicate missing neutrals with invariant mass greater than a π^0 and K^0 respectively.

Table (6b) Reaction Cross Sections for 5-prongs (mb)

reaction	nominal beam momentum (GeV/c)						
	1.0	1.1	1.2	1.3	1.4	1.5	1.6
$\bar{p}n \to 2\pi^+ 3\pi^-$	4.19	3.59	3.66	3.56	3.23	3.16	3.03
	± .22	± .20	± .09	± .13	± .12	± .13	± .12
$\bar{p}n \to 2\pi^+ 3\pi^- \pi^0$	7.79	7.16	7.32	7.16	7.32	6.80	6.81
	± .38	± .35	± .26	± .28	± .29	± .27	± .27
$\bar{p}n \to 2\pi^+ 3\pi^- (mm\pi)$	4.64	4.23	4.83	4.57	4.21	4.47	4.76
	± .33	± .30	± .25	± .26	± .26	± .25	± .25
$\bar{p}n \to K^+ \pi^+ K^- 2\pi^-$	.15	.16	.17	.21	.20	.21	.24
	± .04	± .04	± .02	± .03	± .03	± .03	± .03
$\bar{p}n \to K^+ \pi^+ K^- 2\pi^- \pi^0$							
$\bar{p}n \to K^+ \pi^+ 3\pi^- \bar{K}^0$	.02	0.	.03	.08	.06	.06	.07
$\bar{p}n \to 2\pi^+ K^- 2\pi^- K^0$	± .02	± .01	± .01	± .02	± .02	± .01	± .02
$\bar{p}n \to K^+ \pi^+ K^- 2\pi^- (mm\pi)$							
$\bar{p}n \to K^+ \pi^+ 3\pi^- (mmK)$	0.	.01	.00	.01	.01	.04	.01
$\bar{p}n \to 2\pi^+ K^- 2\pi^- (mmK)$	± .01	± .01	± .01	± .01	± .01	± .01	± .01

1. (mmπ) and (mmK) indicate missing neutrals with invariant mass greater than a π^0 and K^0 respectively.

Table (7) Resonance Fits vs. p_{beam}

reaction	NDF	χ^2	CL	T(2190) (mb)	U(2350) (mb)
3-prong annih.	3	6.1	11%	6.01±2.59	7.86±4.99
$\bar{p}n \to \pi^+ 2\pi^-$	3	1.0	80%	0.56±0.38	0.29±0.49
$\bar{p}n \to \pi^+ 2\pi^- \pi^0$	3	1.8	61%	3.17±1.56	3.89±1.91
$\bar{p}n \to \pi^+ 2\pi^-$ (mms)	3	3.6	31%	1.95±2.47	1.89±5.39
5-prongs	3	6.4	9%	2.26±1.35	5.27±2.89
$\bar{p}n \to 2\pi^+ 3\pi^-$	3	1.8	63%	0.53±0.63	0.97±1.18
$\bar{p}n \to 2\pi^+ 3\pi^- \pi^0$	3	1.5	68%	0.88±1.35	1.60±3.01
$\bar{p}n \to 2\pi^+ 3\pi^-$ (mms)	3	3.9	27%	0.78±1.23	2.54±2.51
$\bar{p}n \to \pi^+ 2\pi^-$ ⎫ $\bar{p}n \to 2\pi^+ 3\pi^-$ ⎭	3	2.5	47%	1.09±0.74	1.35±1.23
$\bar{p}n \to \pi^+ 2\pi^- \pi^0$ ⎫ $\bar{p}n \to 2\pi^+ 3\pi^- \pi^0$ ⎭	3	3.0	39%	3.98±2.16	6.21±3.52

---

1. (mms) indicates missing neutrals with invariant mass greater than a π^0.

2. The amounts of T and U-meson are the fitted values of a_T and a_U respectively.

Table (8) Resonance Fits vs. $E_{c.m.}$

reaction	NDF	χ^2	CL	T(2190) (mb)	U(2350) (mb)
$\bar{p}n \to \pi^+ 2\pi^-$	11	13.3	27%	0.37±0.17	0.02±0.26
$\bar{p}n \to 2\pi^+ 3\pi^-$	11	9.1	62%	0.53±0.26	0.83±0.53
$\bar{p}n \to \pi^+ 2\pi^-$ and $\bar{p}n \to 2\pi^+ 3\pi^-$	11	11.7	39%	0.90±0.31	0.96±0.58

1. The amounts of T and U-meson are the fitted values of a_T and a_U respectively.

Table (9) Beam Momentum Distributions

	nominal beam momentum (GeV/c)						
	1.0	1.1	1.2	1.3	1.4	1.5	1.6
mean value	.999	1.104	1.199	1.291	1.401	1.507	1.605
standard deviation	.018	.019	.016	.016	.019	.025	.023

FIGURE CAPTIONS

1 The unfolded I=1, $\bar{N}N$ cross section from reference (1).

2 Illustration of the topologies scanned for and grouping of the topologies for the purpose of extracting $\bar{p}n$ cross sections. The topologies are grouped so that a short dark stopping proton track is considered a "spectator" of the $\bar{p}n$ interaction.

3 $\bar{p}d$ total cross sections measured by this experiment using the events scanned at each of the three Italian labs separately. Also shown is the more accurate measurement by a high statistics counter experiment whose errors are typically about ±0.15 mb.[1]

4 Our statistical separation of the one-constraint and zero-constraint π-annihilations at each nominal beam momentum. The histograms are combined missing mass spectra of the reactions: $\bar{p}d \to p_s \pi^+ 2\pi^- \pi^0$ and $\bar{p}d \to p_s \pi^+ 2\pi^- (mm\pi)$ for the 3-prongs; and $\bar{p}d \to p_s 2\pi^+ 3\pi^- \pi^0$ and $\bar{p}d \to p_s 2\pi^+ 3\pi^- (mm\pi)$ for the 5-prongs. $(mm\pi)$ indicates missing neutrals with invariant mass greater than a π^0. The curves shown represent the predicted spectra for each reaction and their sum. They are based on the results of our separation.

5 Our shadow corrected 4 and 6-prong cross sections are shown in (a) and (b) respectively ($\sqrt{s}$ = 1.114). For comparison we also show the corresponding $\bar{p}p$ topological cross sections from other experiments.

6 The results of corrections for the shadow effect and loss of long spectator protons for our 3 and 5-prongs. (s = 1.114, $1+f_3$ = 1.30, $1+f_5$ = 1.27)

7 Cross sections vs. nominal beam momentum for the reactions: (a) total 3-prong annihilations, (b) $\bar{p}n \to \pi^+2\pi^-$, (c) $\bar{p}n \to \pi^+2\pi^-\pi^0$, (d) $\bar{p}n \to \pi^+2\pi^-(mm\pi)$, (e) total 5-prongs, (f) $\bar{p}n \to 2\pi^+3\pi^-$, (g) $\bar{p}n \to 2\pi^+3\pi^-\pi^0$, (h) $\bar{p}n \to 2\pi^+3\pi^-(mm\pi)$, (i) the sum of (b) and (f), and (j) the sum of (c) and (g). Curves shown are described in the text. ($mm\pi$) indicates missing neutrals with invariant mass greater than a π^0.

8 Cross section vs. c.m. energy for the reactions: (a) $\bar{p}n \to \pi^+2\pi^-$, (b) $\bar{p}n \to 2\pi^+3\pi^-$ and (c) the sum of (a) and (b). Curves shown are described in the text.

9 Histograms of the invariant mass of π^+p and π^-p combinations in the reactions: (a) $\bar{p}d \to p_s\pi^+2\pi^-$ and (b) $\bar{p}d \to p_s2\pi^+3\pi^-$ for all nominal beam momenta combined. (p_s indicates a stopping proton.) We see a depletion of events in the π^+p mass region around the $\Delta(1236)$.

10 Kinematic limits in E (c.m. energy) vs. p_p (spectator momentum) for (a) the beam momentum p_β = 1.3 GeV/c, (b) for all beam momenta. The theoretical spectator proton momentum spectrum $g(p_p)$ is also shown.

Figure (1)

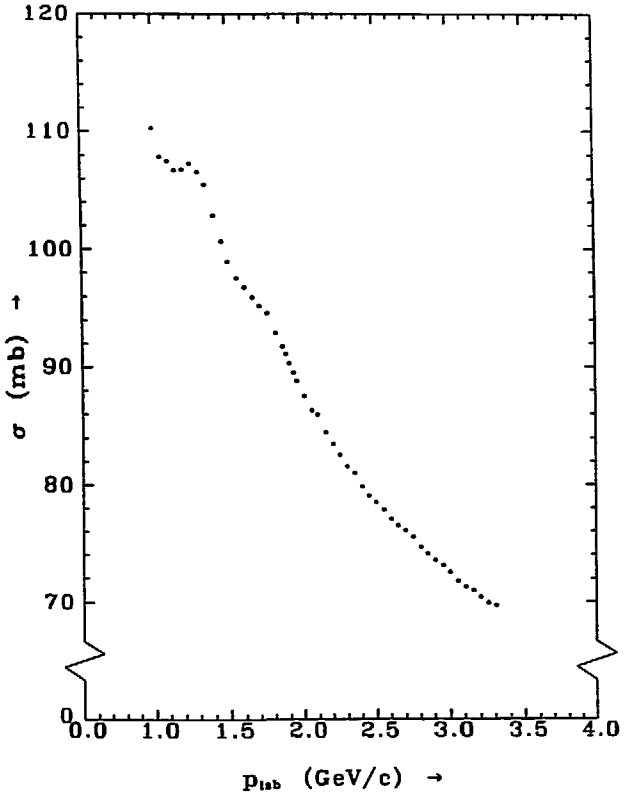

Figure (2)

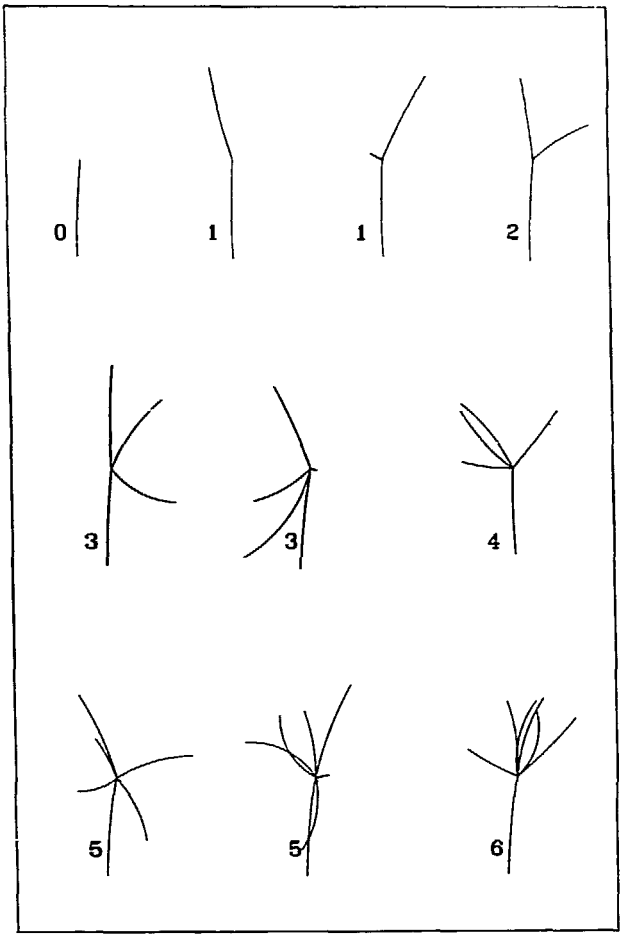

Figure (3)

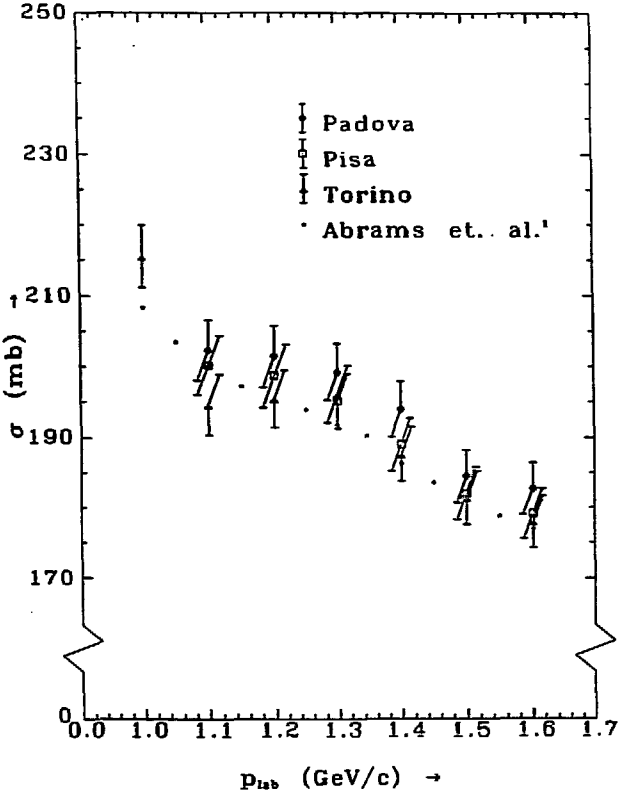
250
230
210
190
170
0
σ (mb)
Padova
Pisa
Torino
Abrams et.. al.'
0.0
1.0
1.1
1.2
1.3
1.4
1.5
1.6
1.7
p_lab (GeV/c) →

Figure (4a) 1.0 GeV/c

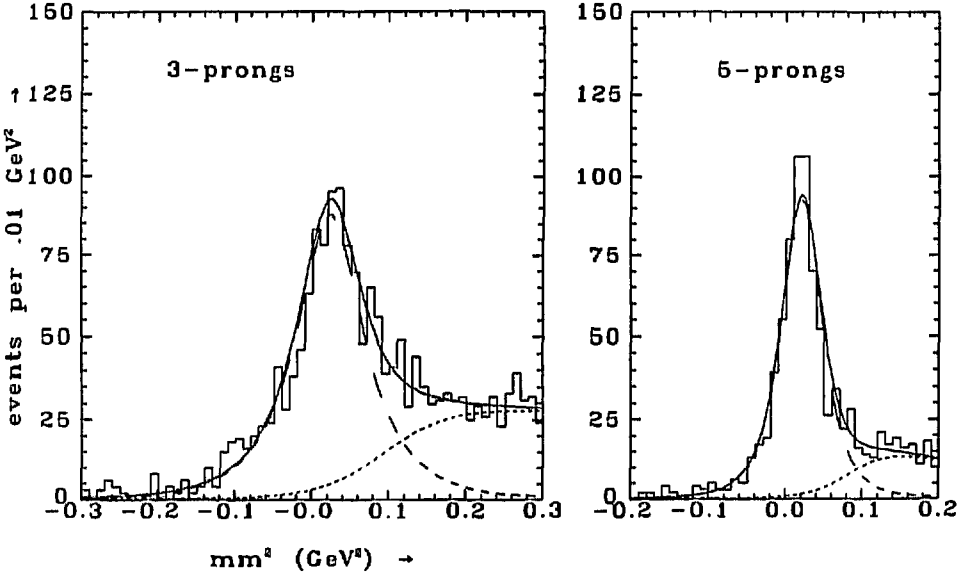

Figure (4b) 1.1 GeV/c

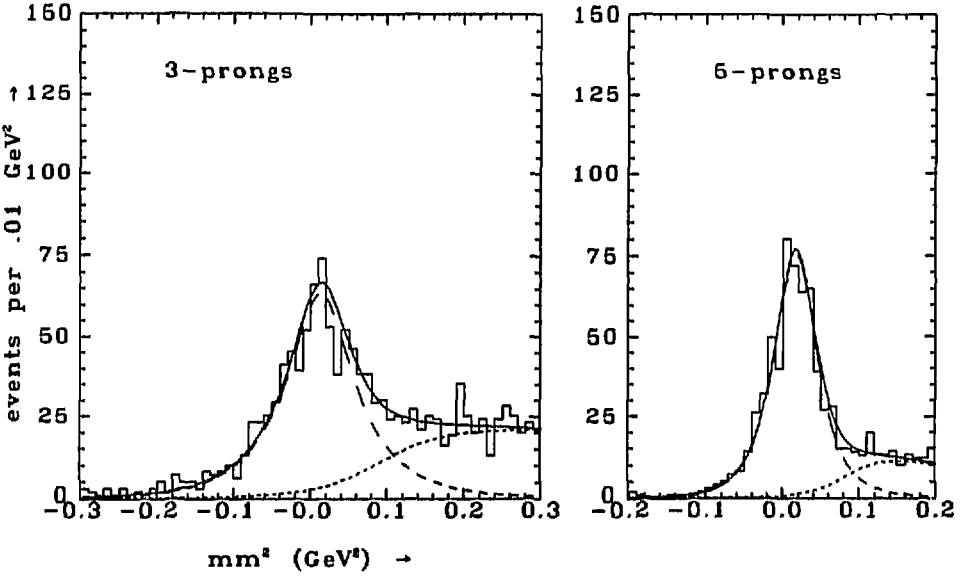

Figure (4c) 1.2 GeV/c

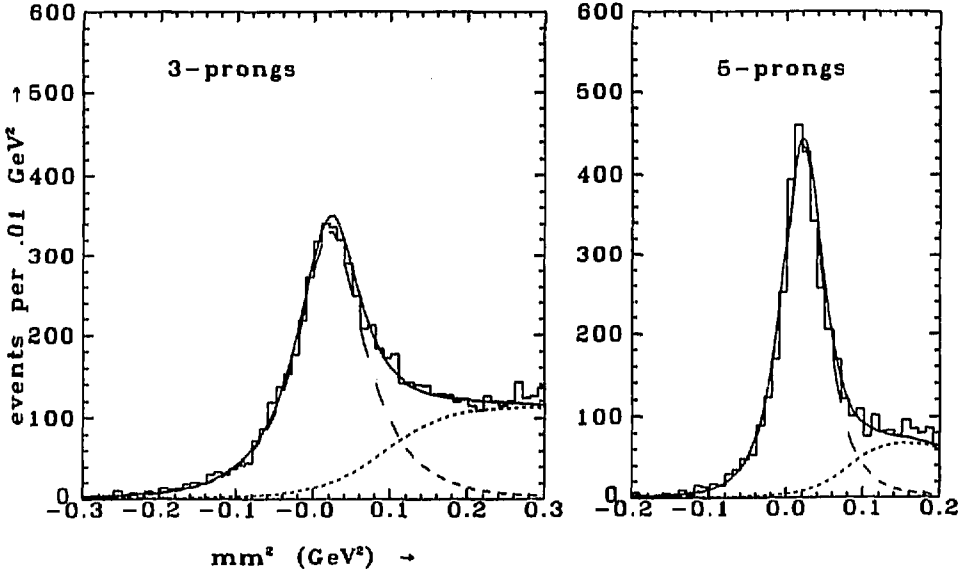

Figure (4d) 1.3 GeV/c

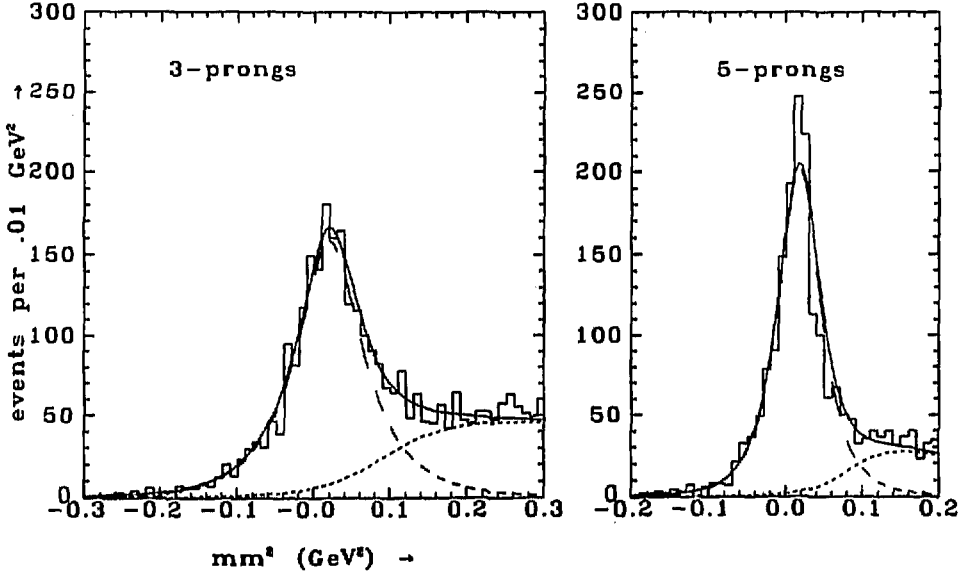

Figure (4e) 1.4 GeV/c

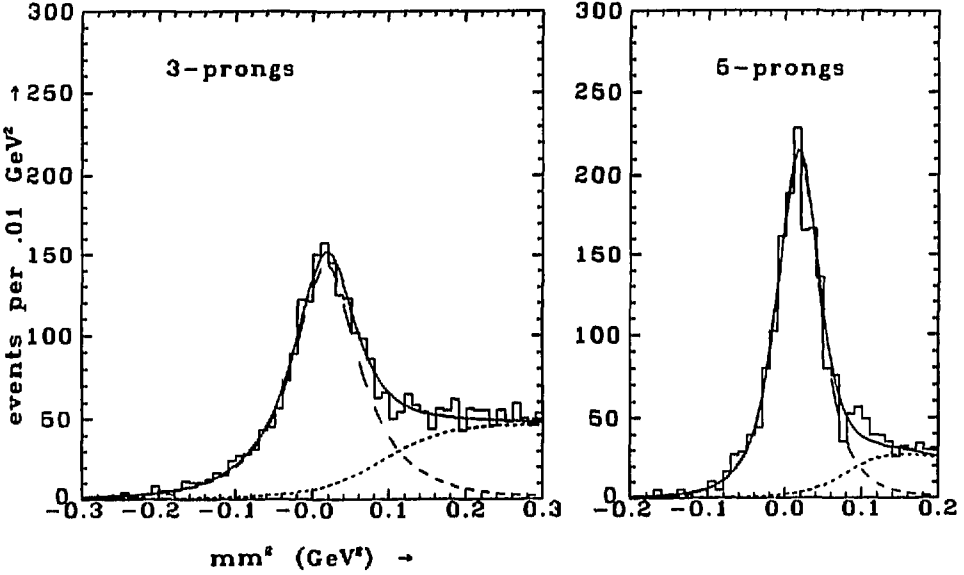

Figure (4f) 1.5 GeV/c

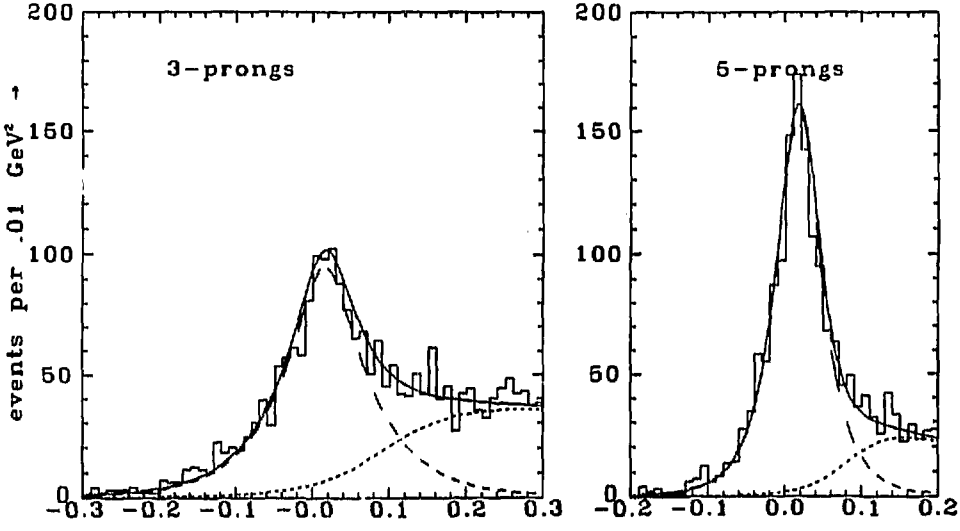

Figure (4g) 1.6 GeV/c

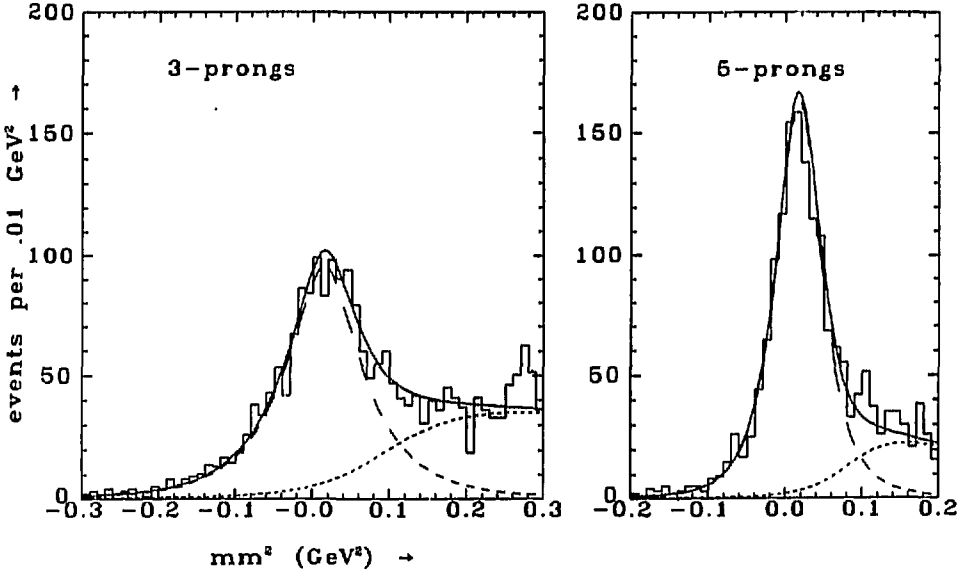

Figure (5a)

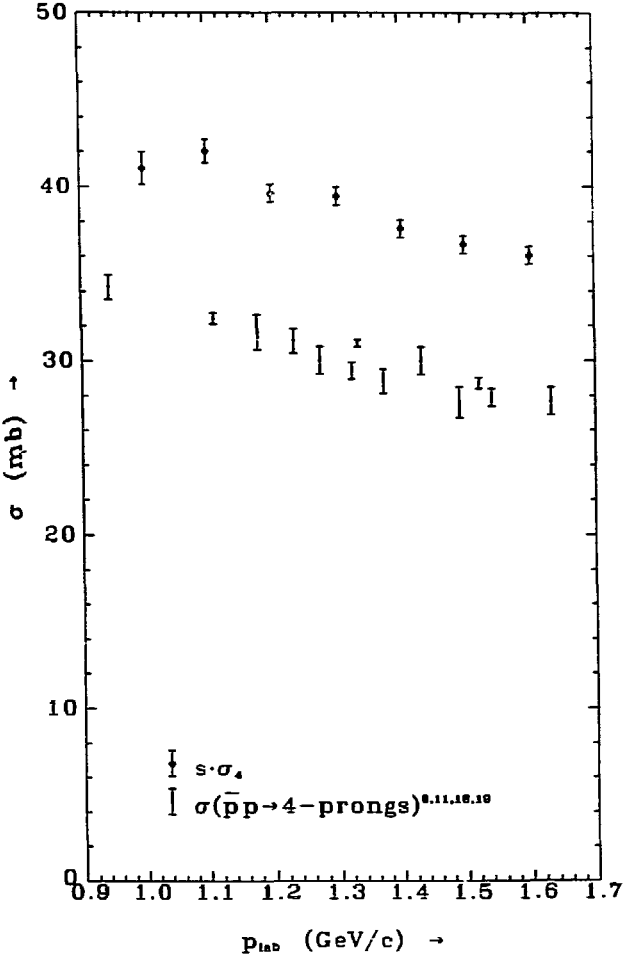
50
40
30
20
10
0
σ (mb) →
0.9 1.0 1.1 1.2 1.3 1.4 1.5 1.6 1.7
p_lab (GeV/c) →
s·σ_4
σ(p̄p→4−prongs)[6,11,16,19]

Figure (5b)

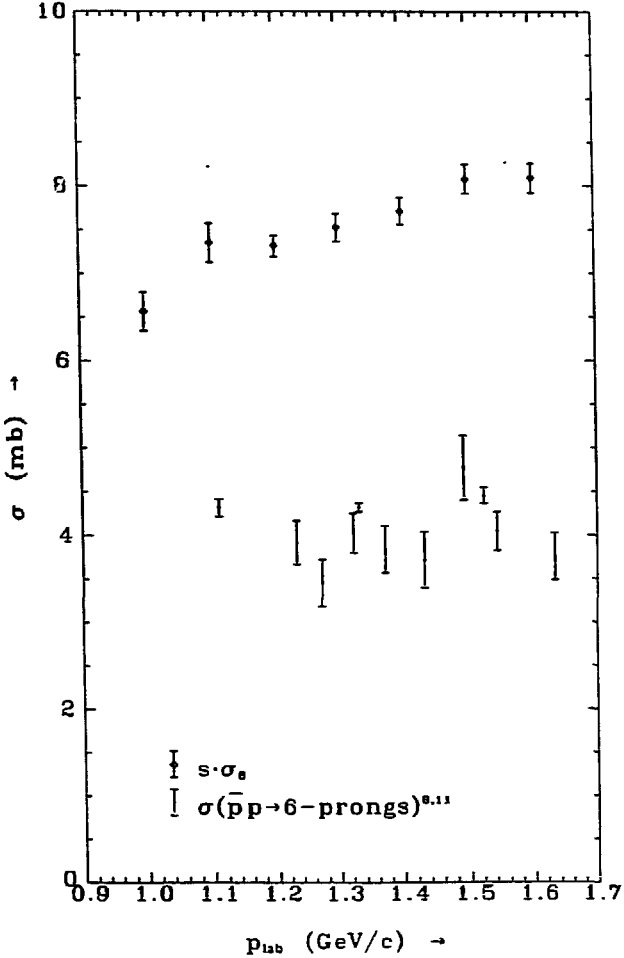
10
8
6
4
2
0
σ (mb) →
0.9 1.0 1.1 1.2 1.3 1.4 1.5 1.6 1.7
p_lab (GeV/c) →
s·σ_e
σ(p̄p→6−prongs)[8,11]

Figure (6)

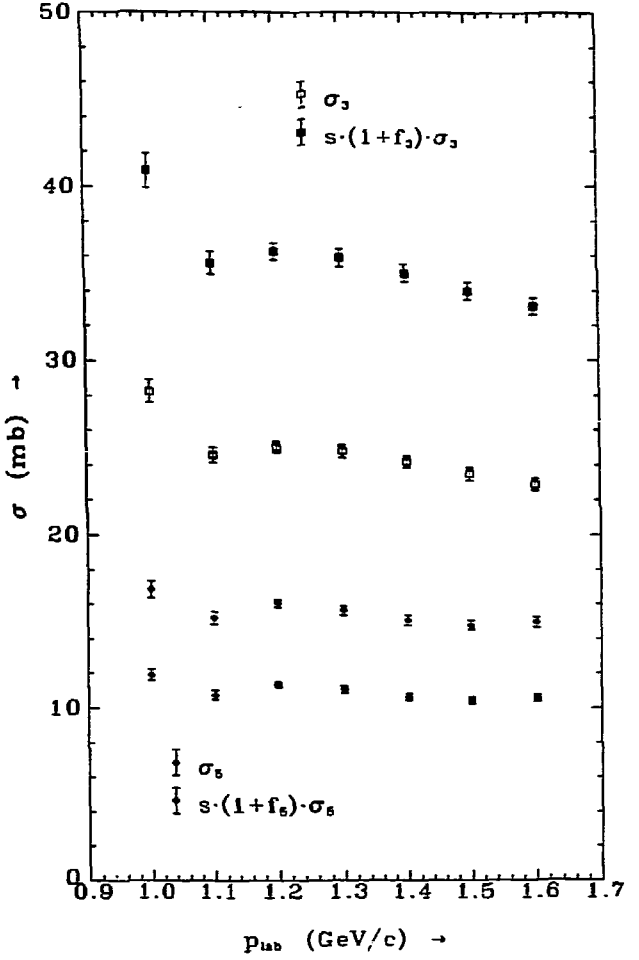
50
40
30
20
10
0
σ (mb) →
σ₃
s·(1+f₃)·σ₃
σ₅
s·(1+f₅)·σ₅
0.9
1.0
1.1
1.2
1.3
1.4
1.5
1.6
1.7
p_lab (GeV/c) →

Figure (7a)

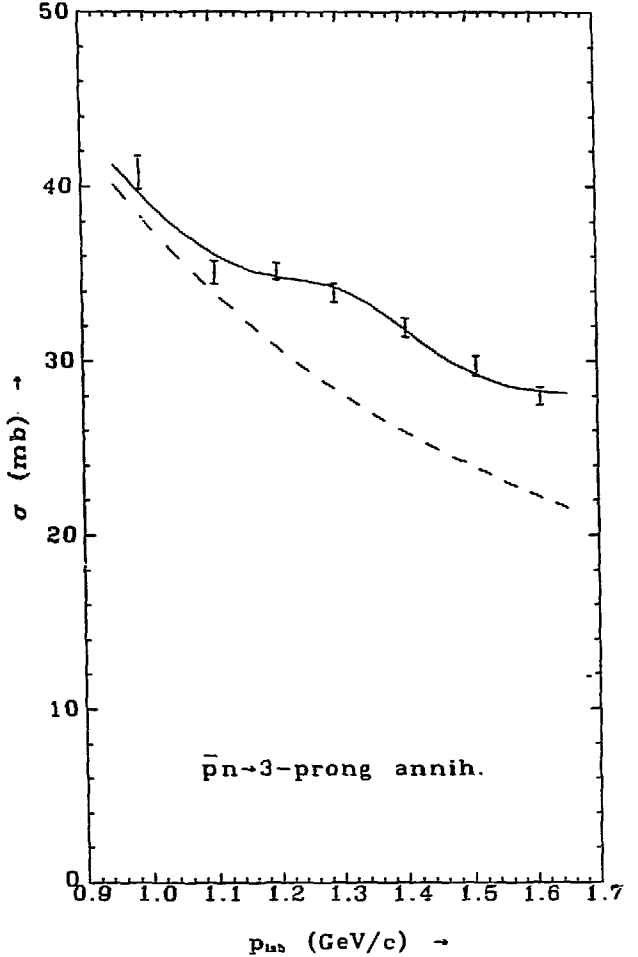
50
40
30
20
10
0
σ (mb) →
0.9 1.0 1.1 1.2 1.3 1.4 1.5 1.6 1.7
p_lab (GeV/c) →
p̄n→3-prong annih.

Figure (7b)

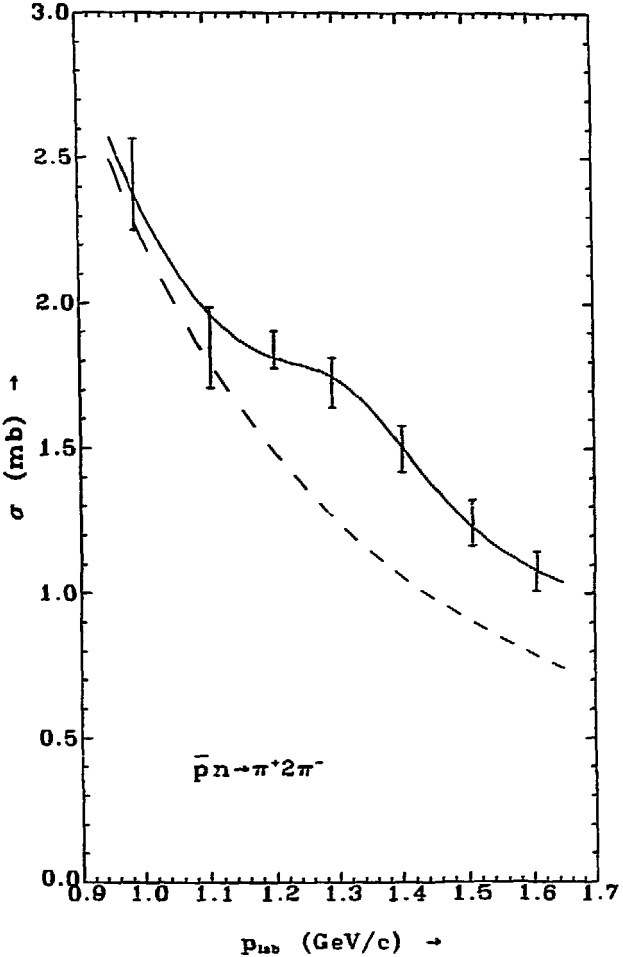
3.0
2.5
2.0
1.5
1.0
0.5
0.0
σ (mb) ↑
$\bar{p}n \to \pi^+ 2\pi^-$
0.9 1.0 1.1 1.2 1.3 1.4 1.5 1.6 1.7
p_{lab} (GeV/c) →

Figure (7c)

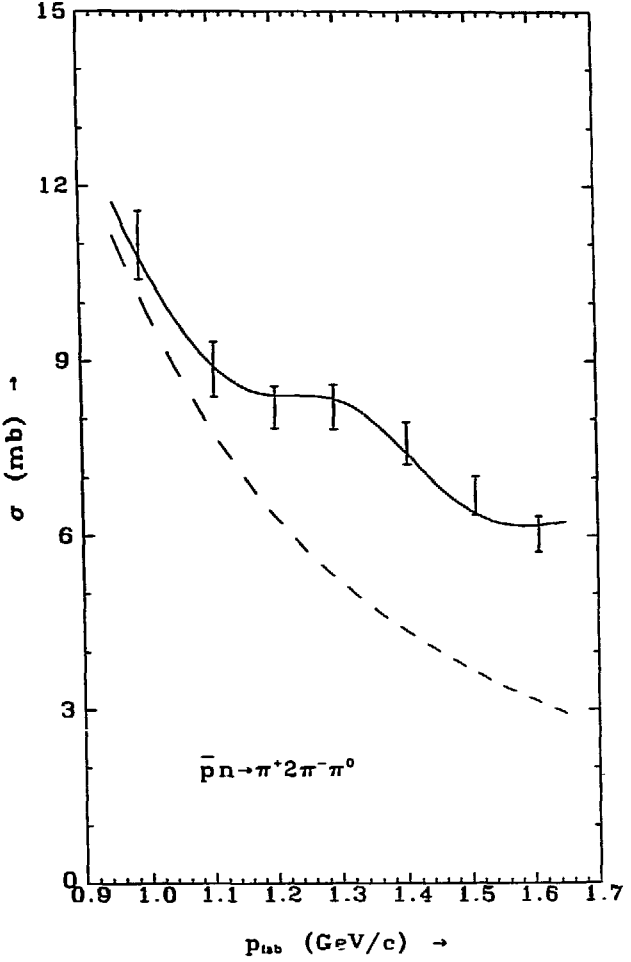
15
12
9
6
3
0
σ (mb) →
0.9
1.0
1.1
1.2
1.3
1.4
1.5
1.6
1.7
$\bar{p}n \to \pi^+ 2\pi^- \pi^0$
p_{lab} (GeV/c) →

Figure (7d)

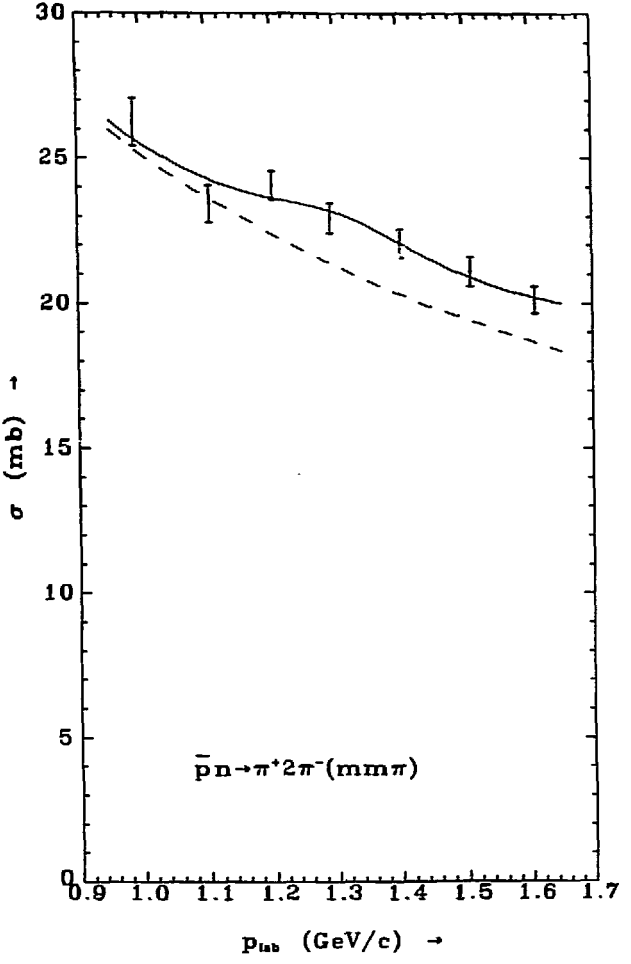
30
25
20
15
10
5
0
σ (mb)
$\bar{p}n \to \pi^+ 2\pi^- (mm\pi)$
0.9
1.0
1.1
1.2
1.3
1.4
1.5
1.6
1.7
p_{lab} (GeV/c) →

Figure (7e)

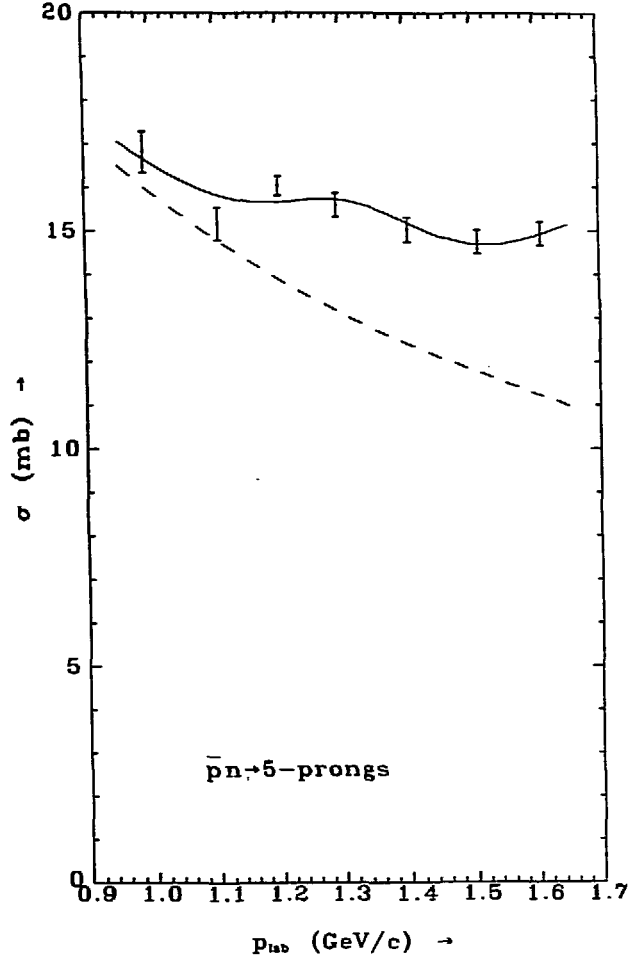

Figure (7f)

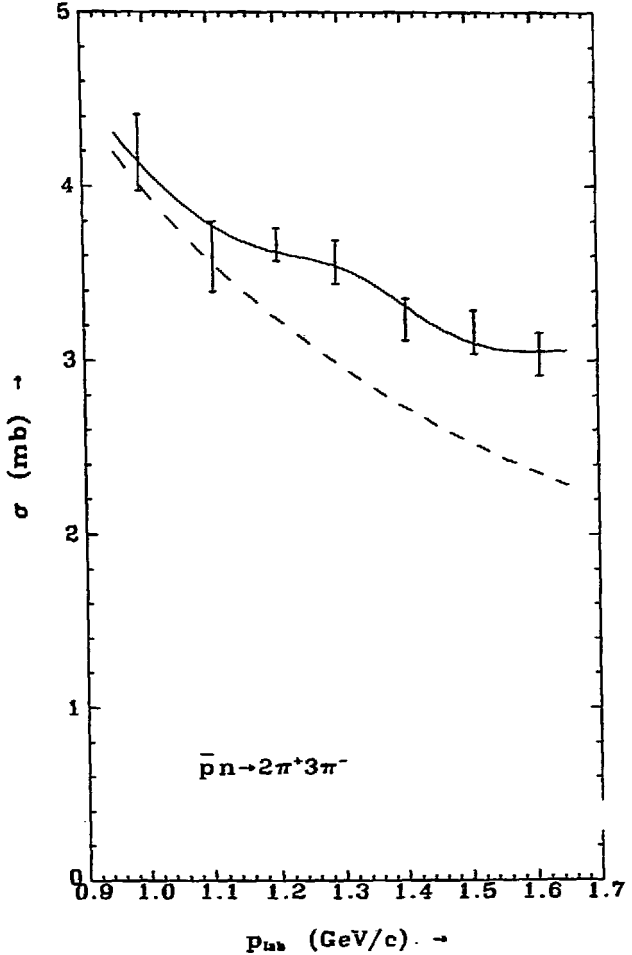

Figure (7g)

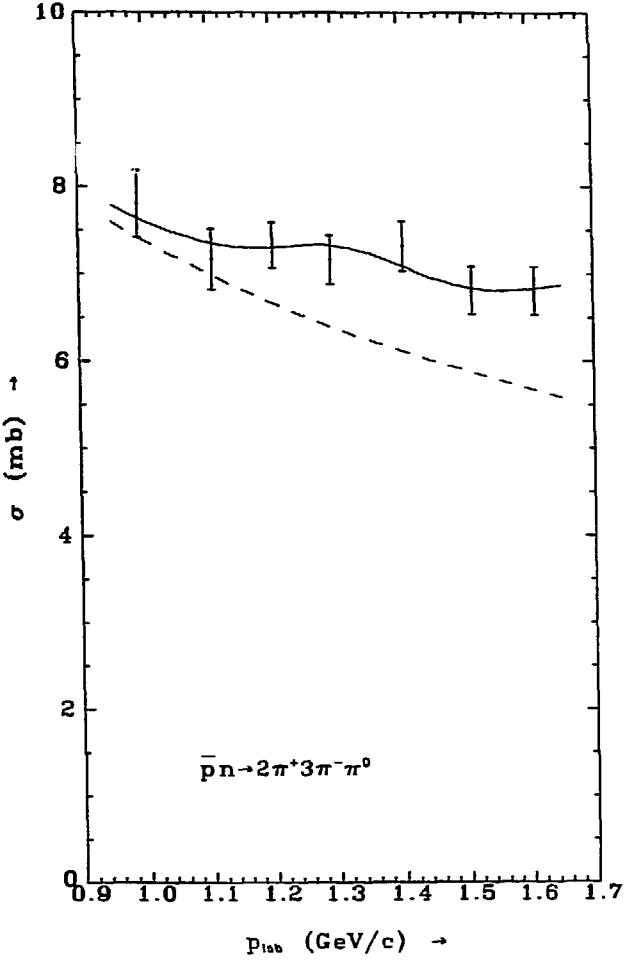
10
8
6
4
2
0
σ (mb)
0.9 1.0 1.1 1.2 1.3 1.4 1.5 1.6 1.7
p_{lab} (GeV/c) →
$\bar{p}n \to 2\pi^+ 3\pi^- \pi^0$

Figure (7h)

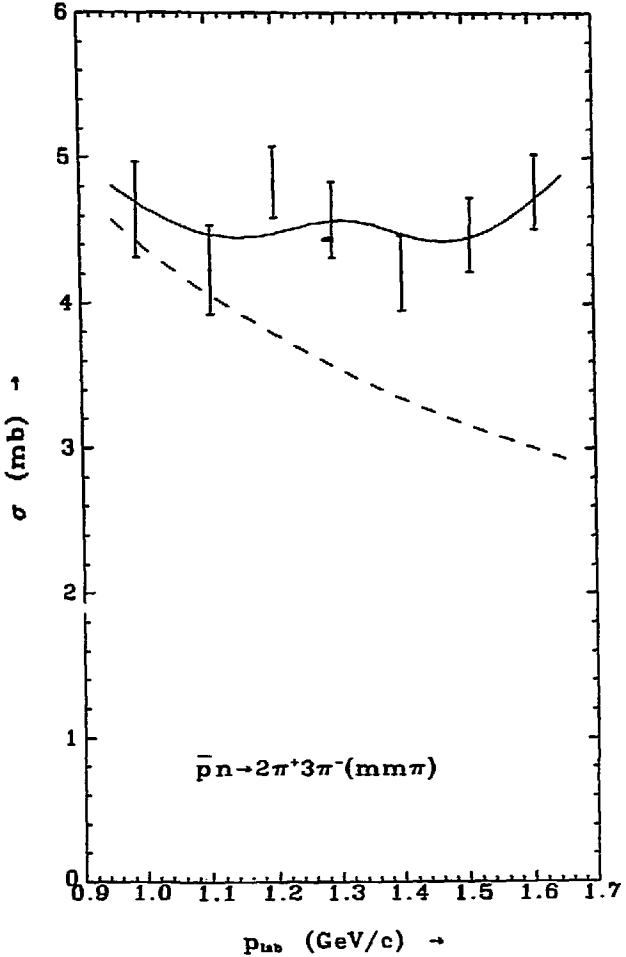
6
5
4
3
2
1
0
σ (mb) →
$\bar{p}n \to 2\pi^+3\pi^-(mm\pi)$
0.9 1.0 1.1 1.2 1.3 1.4 1.5 1.6 1.7
p_{lab} (GeV/c) →

Figure (7i)

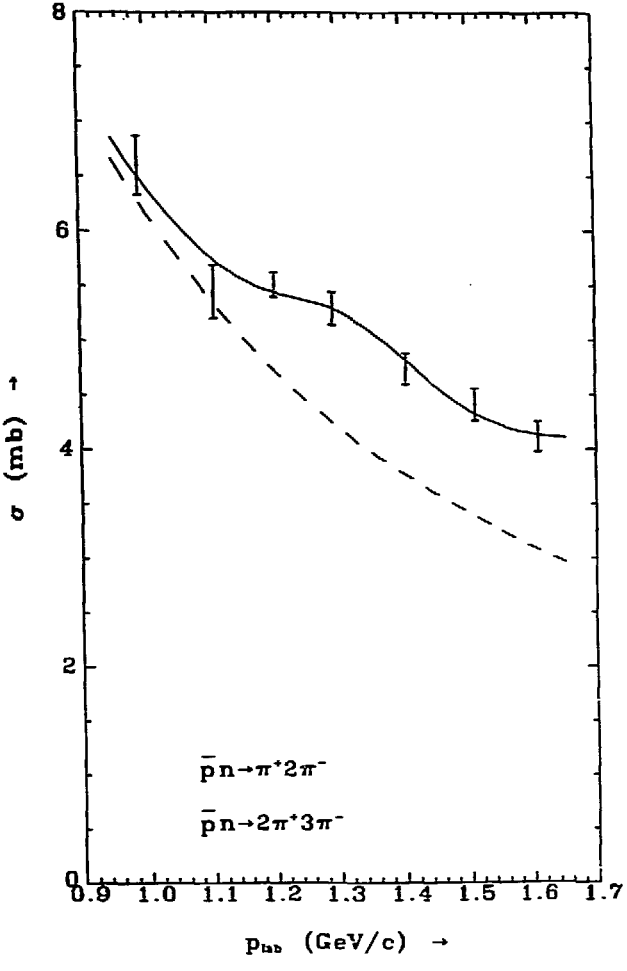

Figure (7j)

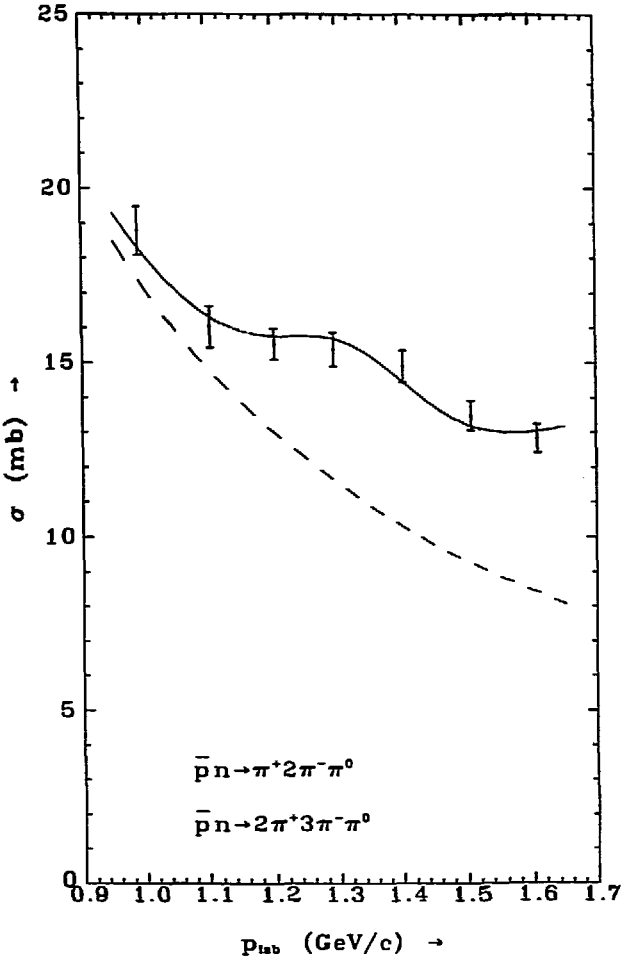
25
20
15
10
5
0
σ (mb) ↑
0.9
1.0
1.1
1.2
1.3
1.4
1.5
1.6
1.7
p_{lab} (GeV/c) →
$\bar{p}n \to \pi^+ 2\pi^- \pi^0$
$\bar{p}n \to 2\pi^+ 3\pi^- \pi^0$

Figure (8a)

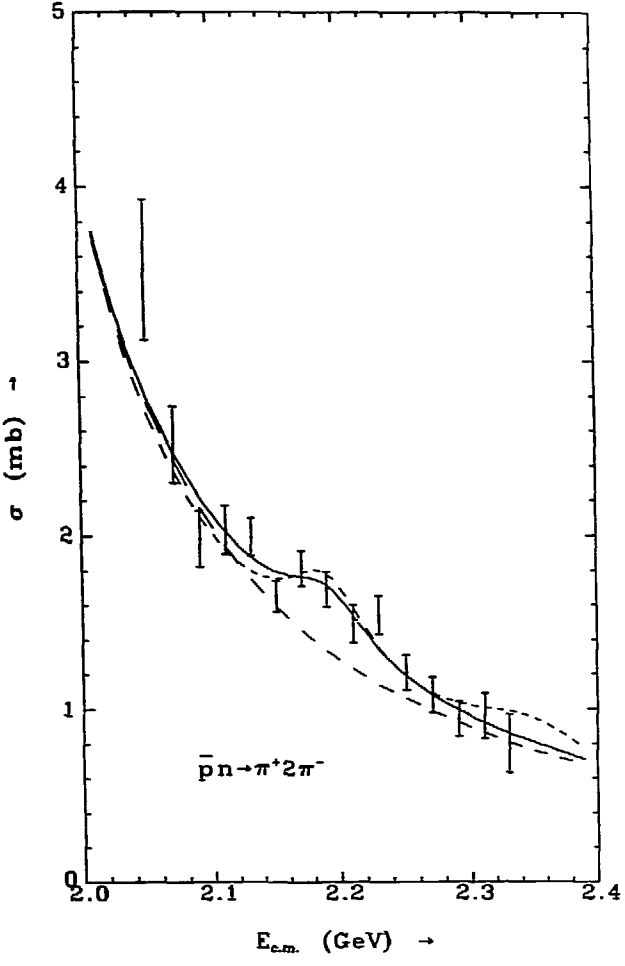

Figure (8b)

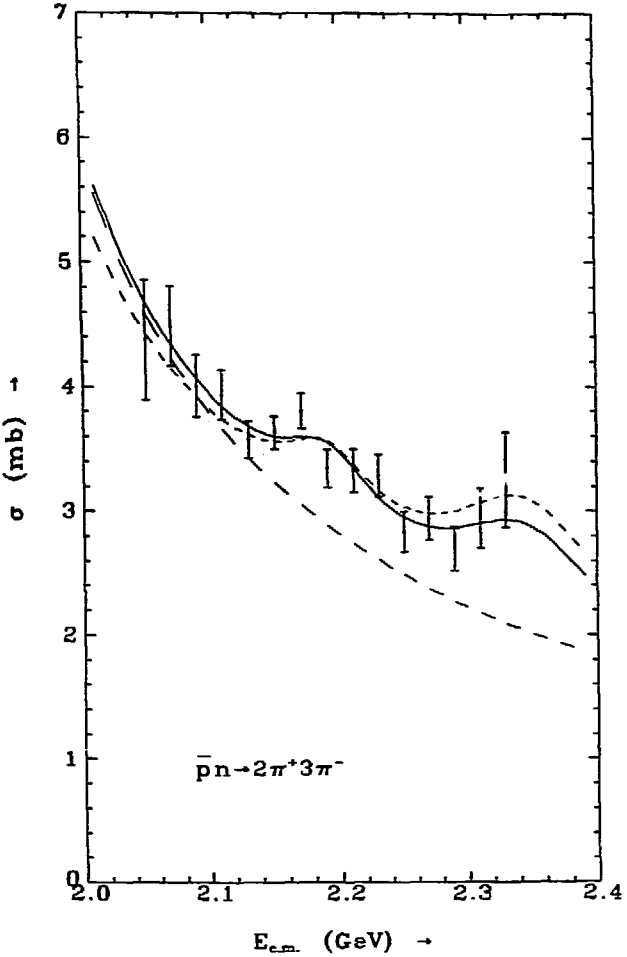

Figure (8c)

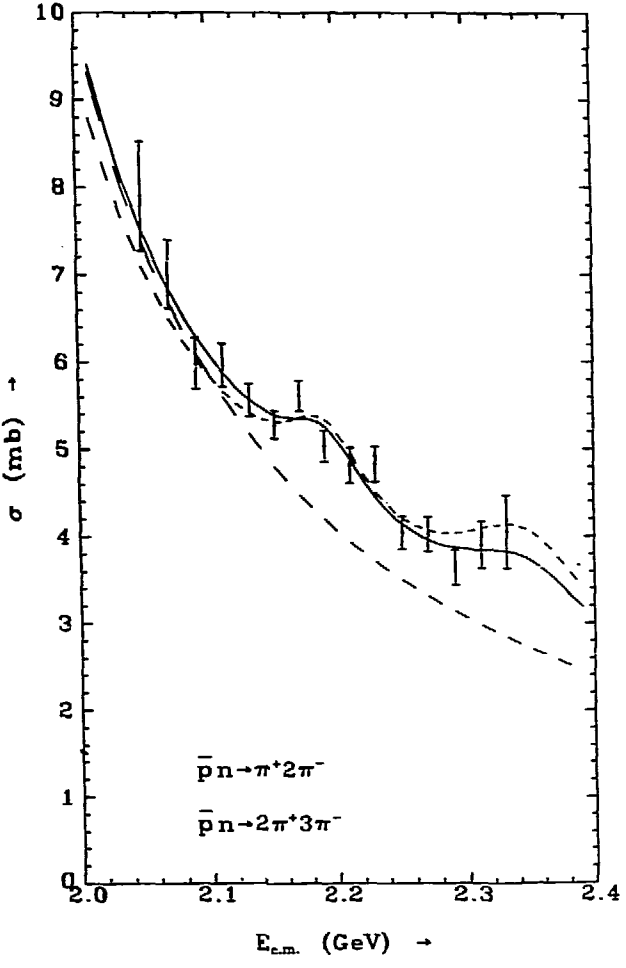

Figure (9a) $\bar{p}d \to p_s \pi^+ 2\pi^-$

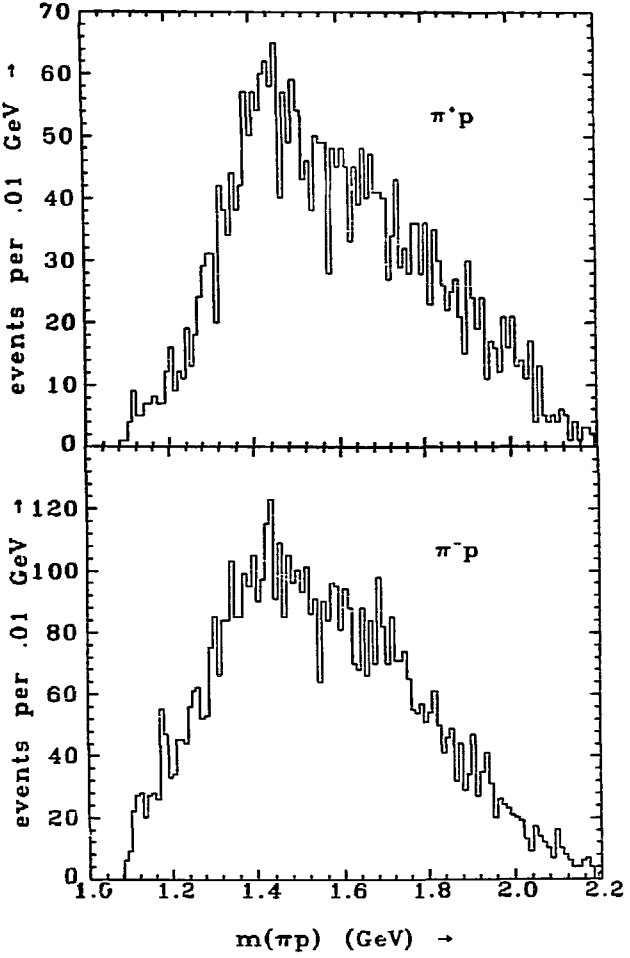

Figure (9b) $\bar{p}d \to p_s 2\pi^+ 3\pi^-$

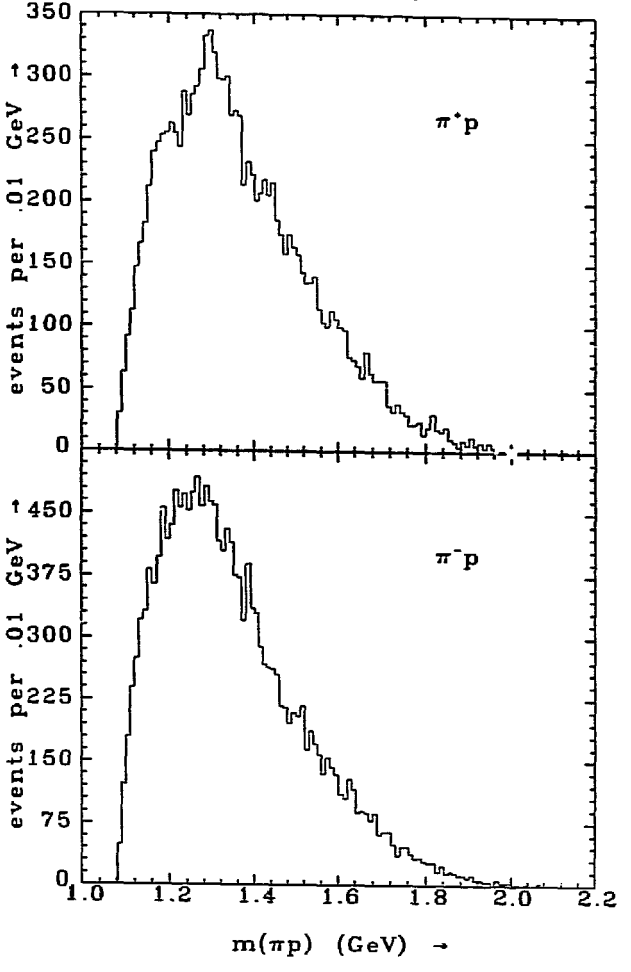

Figure (10a)

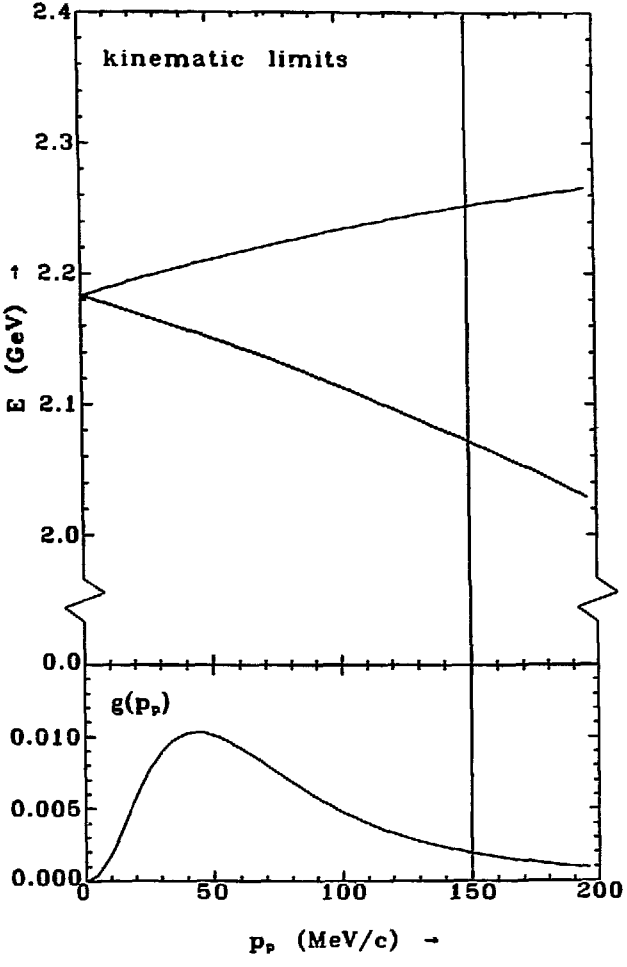
kinematic limits
E (GeV)
2.4
2.3
2.2
2.1
2.0
0.0
g(p_p)
0.010
0.005
0.000
0
50
100
150
200
p_p (MeV/c) →

Figure (10b)

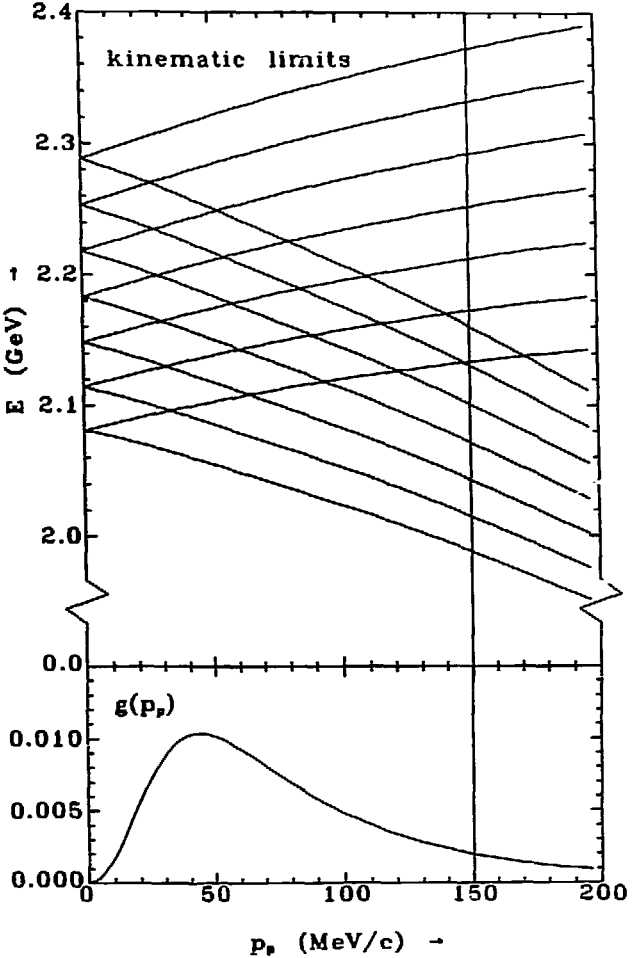
kinematic limits
E (GeV) →
2.4
2.3
2.2
2.1
2.0
0.0
g(p_p)
0.010
0.005
0.000
0
50
100
150
200
p_p (MeV/c) →